Cracking in the concrete foundation for hydropower generators

Part II

Elforsk rapport 13:64

Tobias Gasch, Mattias Nässelqvist, Håkan Hansson,
Richard Malm, Rolf Gustavsson and
Manouchehr Hassanzadeh

September 2013

ELFORSK

Cracking in the concrete foundation for hydropower generators

Part II

Elforsk rapport 13:64

Tobias Gasch, Mattias Nässelqvist, Håkan Hansson,
Richard Malm, Rolf Gustavsson and
Manouchehr Hassanzadeh

September 2013

Förord

Många stora konstruktioner inom vattenkraftindustrin består av betong. Att utveckla och effektivisera förvaltning av dessa är av största betydelse. Genom FoU-insatser ökar möjligheten att genomföra åtgärder vid rätt tid, till lägsta möjliga kostnad och till rätt kvalitet.

Vattenkraftföretagen*) har via Elforsk bedrivit forskning och utveckling inom det betongtekniska området sedan början av 90-talet.

Verksamheten syftar till att utveckla förvaltningen av vattenkraftens betongkonstruktioner för att minska produktionsbortfall orsakade av problem med betongkonstruktioner. Men det finns även en direkt koppling till dammsäkerhetstekniska krav på förvaltningen av betongkonstruktionerna.

Målet är att ta fram verktyg, riktlinjer, utförandebeskrivningar och teknik som fyller industrins behov. Målet är också att bygga kompetens. En uttalad ambition är att samarbeta med övrig industri och landets tekniska högskolor.

Under perioden 2010-2012 har tidigare inriktning mot kraftverkets yttre betongkonstruktioner kompletterats med aggregatnära betongkonstruktioner som utsätts för alltmer dynamisk belastning vid förändrade driftsätt och ökat reglerkraftbehov.

Programmet administreras med hjälp av en styrgrupp som under 2010-2012 bestått av följande ledamöter:

Mats Persson/Erik Nordström/Malte Cederström, Vattenfall Vattenkraft

Johanna Feldtman, E.ON Vattenkraft Sverige

Martin Hansson/Jan Liif, Statkraft Sverige AB

Robert Lundström/Markus Eriksson/Emma Sundelin, Skellefteå Kraft

Stefan Norberg/Karin Persson, Fortum

Marcus Hautakoski/Gunnar Sjödin, Vattenregleringsföretagen

Cristian Andersson/Marie Westberg Wilde, Elforsk AB

Stockholm november 2013

Cristian Andersson

Elforsk AB

*)Vattenfall Vattenkraft AB, Fortum Generation AB, E.ON Vattenkraft Sverige AB, Statkraft Sverige AB, Skellefteå Kraft AB, Jämtkraft AB, Sollefteåforsens AB, Karlstads Energi AB, Jönköping Energi AB deltar i Betongtekniskt program vattenkraft 2010-2012.

Sammanfattning

Ett kontinuerligt arbete med utvärdering och uppgradering av vattenkraften pågår i Sverige. Syftet är att säkerställa långvarig och säker drift av vattenkraftens konstruktioner ur ett byggnadstekniskt perspektiv.

Vid inspektioner av svenska vattenkraftsstationer har, i vissa fall, sprickor observerats i de betongfundament som utgör generatorns upplag och i synnerhet kring stator- och rotorupplagen. En av de bidragande orsakerna till dessa sprickor tros vara dynamiska påkänningar som orsakas av ett nytt driftsmönster, samt även andra dynamiska påkänningar. Dessa dynamiska påkänningar kan utgöras av lastfrånslag/snabbstopp och ökade dynamiska laster vid övervarvning, samt även sällan förekommande påkänningar som t.ex. kortslutning av generatorn. Tidigare användes generatorerna kontinuerligt medan vattenkraften idag används för att balansera energitillförseln, vilket leder till många starter och stopp, ibland under ett och samma dygn.

Syftet med föreliggande projekt är att förstå den komplicerade samverkan mellan generator (stator, rotor, turbin, etc.) och betongkonstruktionen som utgör generatorns upplag för att kunna bestämma orsaken till de sprickor som observerats i fält, samt att kunna prediktera både sprickor i betongfundament och framtida underhållsbehov.

En tredimensionell finita-elementmodell av ett generatorfundament har definierats i ett tidigare projekt och denna modell har använts för utvärdering av metodik för analyser av interaktionen mellan betongkonstruktionen och generatorn. Inverkan av sprickor i fundamentet har studerats baserat på beräknat sprickmönster erhållet vid tidigare genomförda FE-analyser. Dessa analyser visade att uttorkningskrympningen huvudsakligen orsakar uppsprickning på fundamentets insida och främst vid upplagen för stator- och rotorbalkar. Dessa analysresultat användes som indata för denna studie, varvid fundamentets ändrade egenstrukturella beteende och dess inverkan på fundamentets interaktion med generatorn har beaktats med hänsyn till effekter från egentyngder och driftsbelastningar.

Resultatet från projektet visar att analyser av strukturinteraktion mellan en generator och ett betongfundament kan genomföras med hänsyn tagen till sprickornas geometri. Detta spricksystem kan vara bestämt med hjälp av FE-analyser, eller baserat på befintliga sprickor för ett specifikt betongfundament. Resultaten visar att fortsatta studier krävs avseende samverkan mellan de termomekaniska laster, inverkan av uttorknings-krypning och krympning för betongen under långtidsbelastning, samt dynamiska lasteffekter orsakade av generatorn. Detta då samverkan av de olika belastningarnas antagligen resulterar i ökade påfrestningar på betongfundamentet. Dessa analyser bör genomföras med ökad geometrisk upplösning avseende betong- och stödstrukturens uppbyggnad, detta för att möjliggöra analyser av lokala spänningsvariationer vid fundamentets perforationer och generatorns upplag. Den aktuella problemställningen kommer att beaktas inom ett doktorandprojekt vid KTH, med stöd av SVC Svenskt VattenkraftCentrum.

Summary

An extensive program for improvement of the hydropower plants in Sweden is currently on-going. The aims are to secure future production and to maintain and further develop an already high dam safety.

During inspection, cracks were discovered in the concrete foundation, near the stator and rotor spider supports, at some hydropower stations in Sweden. The cracks were believed to be related to new patterns for generator operation, thereby changing the dynamic loading of the stator and rotor spider supports. Previously the generators ran continuously, while nowadays there are an increased number of stops and starts, sometimes even several times during one day. Increased dynamic forces due to runaways, and also other dynamic events such as emergency stops, may also contribute to increased stress levels and cracking of the foundation. Furthermore, although extreme loads such as short circuits of the generator seldom occurs, the influence on the dynamic forces acting on the supporting structure and concrete foundation may be strongly influenced during such events.

The objective of this study is to understand the complex interaction between the power generating system (stator, rotor, turbine, etc.) and its supporting concrete structure to determine the causes of existing structural cracks in the foundation. Furthermore, to be able to predict further crack propagation of the concrete foundation will help to determine future maintenance requirements.

A three dimensional non-linear finite element model developed earlier was used to evaluate a methodology for analyses of the interaction between the generator and the concrete foundation. The influence of cracks in the concrete foundation was investigated by including the fracture pattern obtained in earlier FE analyses of time-dependent thermal and moisture gradients. These analyses showed that the drying shrinkage induced cracking inside the concrete foundation and especially close to the supports of the stator and the rotor spider. The obtained fracture pattern for the previous analysis was used as input for this study, with the concrete foundation's changed structural properties and their influence on the interaction with the generator considered in the analyses. Furthermore, deadweight and operational load were also included in the analyses.

The study show that FE models with a cracked concrete foundation can be used to analyse structural interaction between foundation and generator components during operation of a hydro power generator. The crack pattern can be determined by FE analyses, or by in-situ measurements of existing concrete cracks for a specific concrete foundation. The analyses show that further studies are needed regarding the combined effects from thermo-mechanical loads, drying shrinkage, creep and dynamical loads caused by the generator. The combined effects may further increase the stress levels for the concrete foundation, especially locally near perforations, and stator and rotor spider supports. These analyses should be performed with an increased numerical resolution for both the concrete foundation and the supporting structure for the generator, with an increased accuracy for the local stress variations near perforations of the foundation and also at the supports for the generator. This research area will be further investigated within a recently started research project at KTH, financed by the Swedish Hydropower Centre.

Contents

1 Introduction

1.1 Background

A rather extensive program for improvement of the Swedish hydropower plants is on-going. The aims are to secure future production, and to maintain and further develop an already high dam safety.

Almost all electricity production involves rotating machinery, an important part of the system for converting potential energy or kinetic energy into electrical energy. At a hydropower plant, the runner converts the potential energy stored in the reservoir into kinetic energy. The turbine is connected via a shaft to a generator which turns kinetic energy into electrical energy.

These transformations give rise to radial, tangential and axial forces which are propagated further into the concrete structure of the unit. The design flow and head affect the choice of generator design and runner type. The designers of the hydropower units have selected different design solutions depending on manufacturer, age and size of the hydropower unit in question. In the field of Swedish hydropower, at least 90% of the large hydropower units have Francis or Kaplan runners. Pelton and Bulb are other runner types which are relatively common elsewhere. The Pelton turbine is used where there are high heads. This is an impulse turbine, which means that it does not give rise to any axial load besides its own weight and has a relatively low mass and high rotational speed. The Bulb turbine is horizontal, and the generator is positioned in the waterway. Radial and axial loads from the turbine and generator are transferred primarily to the surrounding structure by means of a stay ring and stay cones (Raabe, 1985). The self weight of the system is largely carried by the Bulb's displacement.

Experience from earlier reports in this field has indicated that cracks may occur at the points where loads from the unit are transferred into the concrete structure. These cracks may be caused by incorrect design of the foundations, incorrect estimation of design loads, mechanical connections in the supporting structure failing to perform the function for which they were designed, or incorrect maintenance of components leading to increased load levels.

If the unit's operating modes are changed, this also impacts upon the loads occurring in the unit and affects the surrounding structure (i.e. more starts and stops, more power regulations, operation outside the best efficiency range with changes in load levels).

The non-linear finite element method was used for earlier studies of structural behaviour of large concrete structures, e.g. Malm et al. (2013). The study in this report is a continuation of previous projects, aiming at applying the method to analyse the dynamic load on concrete foundations for hydro power generators.

The objective of this project is to enhance the understanding of the complex interaction between the power generating system (stator, rotor, runner, etc.) and the supporting concrete structure, which is needed for formulation of more realistic and accurate specifications regarding load, stiffness and displacement levels and tolerances. The various loading condition includes

- mechanical loads (static, dynamic, short-term, long-term, etc) such as weight of the structures and systems, and operating loads caused by the turbine, rotor, stator, etc
- environmental loads (physical, chemical, etc) such as strains and restraints caused by temperature, moisture variations, and chemical reactions.

The study presented in this report focus on the dynamic load induced by a rotating hydro power generator on the concrete structure.

1.2 Project organisation

The project group consists of representatives from KTH (The Royal Institute of Technology), Vattenfall Engineering and ÅF. The project is financially supported by Elforsk AB, the Swedish Power Companies R&D association.

The project is coordinated by adjunct Prof. Manouchehr Hassanzadeh from Vattenfall Engineering, who also contributed with knowledge on material formulation and fracture mechanics for concrete. From the department of Concrete Structures at KTH, Dr. Richard Malm contributed by developing the structural models and with knowledge regarding advanced numerical simulations. He is also responsible for the formulation and evaluation of the numerical results presented in this report. Ph.D. candidate Tobias Gasch from the department of Concrete Structures at KTH and Vattenfall Engineering, together with tech. lic. Håkan Hansson from the department of Concrete Structures at KTH contributed with knowledge on advanced numerical simulations and non-linear material properties. Together, they performed all numerical analyses that are presented in this report and have written most of the report. Dr. Mattias Nässelqvist from ÅF and Dr. Rolf Gustavsson from Vattenfall Engineering have contributed with knowledge regarding the generator and its loads. In addition, they have also written chapter 2 and 3 of this report regarding the generator support structure and its components as well as the loads generated by the hydropower unit.

2 Hydro power generator support structure and components

The loads which the rotating system gives rise to are absorbed by axial and radial bearings: these are then propagated via the supporting structure out to the concrete structure. Components shown in orange and red in Figure 2—1 are rotating parts, with the support structure shown in pink.

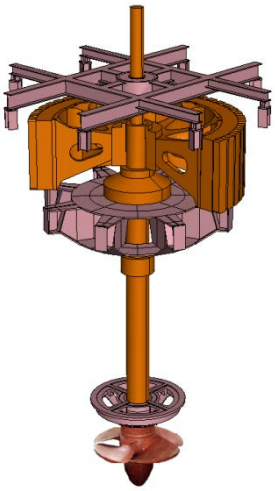

Figure 2—1: Schematic diagram of a hydropower unit.

The design solutions for the hydropower unit are dependent on the manufacturer, age and size of the hydropower unit. Axial and radial loads are caused by the turbine, generator, shaft system and supporting structure. The units have two or three radial bearings and one axial bearing in order to absorb the loads occurring in these components and hold the rotating system in position. How these bearings and supporting structures are positioned in relation to other machine components varies, but in Sweden more or less all large units have one of the configurations shown in Figure 2—2. The solid square represents a radial bearing and a clear square represents an axial bearing.

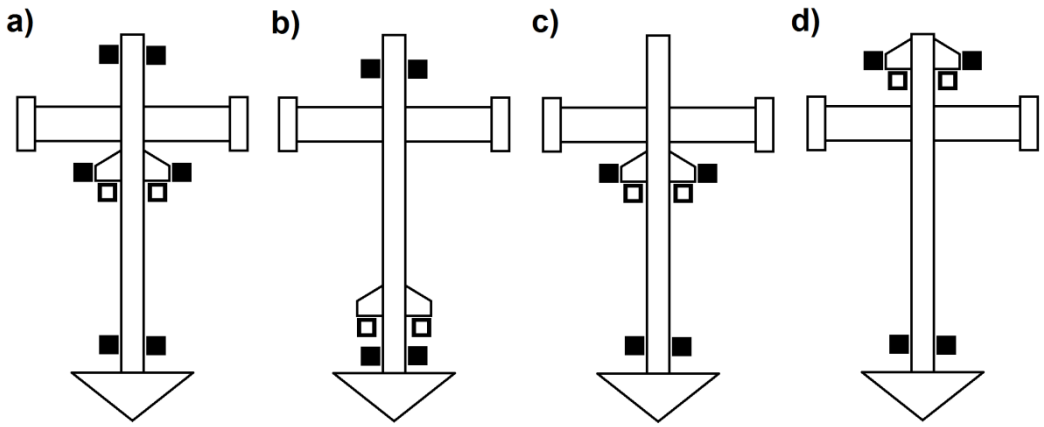

Figure 2—2: Schematic layout for bearings and supporting structure.

In Sweden, a majority of the hydropower units are of type **a** shown in Figure 2—2, but the large units (>200 MW) in Sweden are of type **b**. Most of the radial loads arising at the runner are absorbed by the radial turbine guide bearing, and most of the radial loads arising at the generator are absorbed by the generator radial guide bearing / bearings. Why the designers of the large Swedish units have decided to use only one generator guide bearing is unknown, but this does mean that high loads can occur at these bearings, their supporting structure and their attachment to the concrete structure.

Mechanical, electrical and thermal loads occur in the generator. The loads which should be taken into account at the runner are hydraulic and mechanical loads. The forces occurring between the rotating and the static system in the turbine and generator are absorbed by the surrounding bearings presented in Figure 2-2 and supporting structure. These are then propagated to the concrete structure.

Vibration monitoring of the units is used widely in order to protect the units and prevent damage occurring during normal operation. Vibration monitoring is also used as a tool in order to determine the need for maintenance and to protect against unit degeneration and overload. Knowledge of which loads which affect components and the surrounding structure in different operating situations is vital so that the unit can be designed correctly and so that component degeneration can be assessed in order to prevent malfunctions.

2.1 Generator

Generator sizes over the past century have increased from a few hundreds of kW to several hundreds of MW. The development and size increase in generators' intended for hydropower production have resulted in a need for development of the hydro power technology. An increase in the efficiency of generators and turbines, new types of bearings and new types of materials have been introduced to the design, and these represent important steps in this development process.

2.1.1 Mechanical loads

The mechanical loads that occurs in the generator are caused by mechanical unbalances. A balance quality grade of G6.3 is required for new and refurbished units, which means that the unbalance force (F) of the generator rotor can be calculated as follows:

$$F = me\Omega^2 = \frac{m6.3\Omega}{1000} \quad (1)$$

where m is the mass of the generator rotor, e is the permissible residual specific unbalance and Ω is the angular velocity. The force follows the rotor speed, which means that the load at a given support point will vary harmonically with the rotational speed. The rotor's unbalanced forces are relatively small if the rotor meets the balancing requirements, as shown in the following example:

A rotor weighing 200 metric tons which rotates at 166.7 RPM and is balanced to G6.3 means that the unbalance force (F) caused by rotor eccentricity is 22 kN, and this force must be distributed between the generator bearings.

The unit's thrust bearing holds up the weight of the rotating parts in the unit plus the water load which acts on the turbine. Vertical additional forces from the generator under normal operation are negligible, but the rotating system can load the axial bearing due to its weight in the event of transients from the turbine, e.g. in the event of water hammer.

2.1.2 Electromagnetic loads

Electromagnetic forces occurring in the unit and affecting the surrounding structure can be divided into two cases, radial forces and tangential forces. The electromagnetic radial force, *UMP* (Unbalanced Magnetic Pull), is due to the fact that the rotor and stator are not concentric with one another, while the tangential force is dependent upon the power output from the generator.

The electro-magnetic pulling force acting on the generator rotor depends on the asymmetry in the air gap between the rotor and stator. In a perfectly symmetrical machine the radial pulling forces should add up to zero. However, all practical generators have some asymmetry in the air gap (Sadarangani, 2006). A common example of asymmetry is when the rotor center and stator center do not coincide with each other. The relative eccentricity is defined as:

$$\varepsilon = \frac{e}{\Delta R} \quad (2)$$

where e is the radial displacement of the rotor center and the average air gap ΔR is the radial clearance between the inner radius of the stator (R_s) and the outer radius of the rotor (R_r) The rotor eccentricity can be sketched schematically as shown in Figure 2—3.

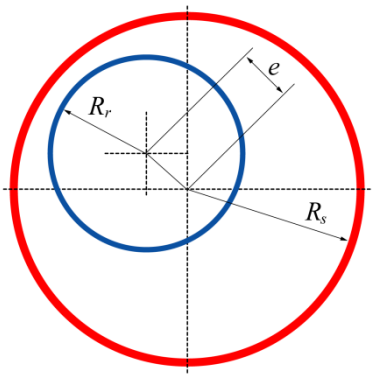

Figure 2—3: Schematic sketch of the air gap with an eccentric rotor.

Belmans et al. (1982) and Sandarangani (2006) have shown that in a three-phase electrical machine with an arbitrary number of poles, the magnetic pulling force is composed of a constant element and an alternating element. The alternating element of the force alternates at twice the supply frequency for static eccentricity, and twice the supply frequency multiplied by the slip for dynamic eccentricity. Sandarangani (2006) showed that the alternating force component decreases as the number of poles in the generator increases. Hydropower generators usually have many poles and operate as synchronous machines. This implies that the alternating magnetic pulling force is negligible in comparison to the constant magnetic pulling force. The expression for the value of the constant unbalanced magnetic pulling force (F_e) for a rotor parallel to the stator was found from the integration of the horizontal and vertical projection of the Maxwell stress over the rotor surface. The mean value of the magnetic pulling force can be expressed as follows:

$$F_e = \frac{\mu_0 S_s^2 R_s^3 h\pi}{2p^2 \Delta R^2} \frac{\varepsilon}{\sqrt{\left(1-\varepsilon^2\right)^3}} \tag{3}$$

where S_s is the stator's linear current density, p is the number of pole pairs, h is the length of the rotor and μ_0 is the permeability of free space. The result of Equation 3 is that the magnetic pulling force is a non-linear function of the air gap eccentricity and the magnetic pulling force will destabilize the rotor system with increasing rotor eccentricity.

The air gap eccentricity can be divided into two categories; stator eccentricity and rotor eccentricity. In the case of stator eccentricity, the rotor will be in a fixed position relative to the stator under a constant magnetic pulling force. This means that the smallest air gap will remain in the same direction during rotation of the shaft. Characteristic of rotor eccentricity is the fact that the rotor will whirl around the center line of the rotor in an orbit. However, the most common case of eccentricity is a combination of stator and rotor eccentricity, and the rotor center will whirl around a fixed position in the stator bore with the angular speed of rotation (Gustavsson et al., 2012). Figure 2—4 presents the measured radial force at a generator guide bearing.

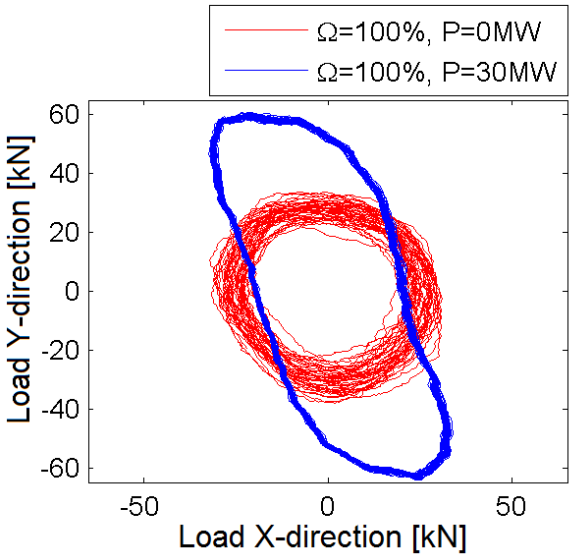

Figure 2—4: Measured radial load at generator guide bearing at 0 and 70% power.

2.1.3 Thermal loads

Older units have cast stator frames in many instances which are bolted to the foundation. This means that the foundations have to absorb both a radial load and a torque caused by the heating of the stator. The size of the load on the foundations is dependent on – among other things – how the stator is designed, how high the temperature increase is in the stator frame and the stiffness of the surrounding structure. The stator will expand more quickly than the foundation when the temperature increases, which means that the foundation will counteract the movement of the stator. This means that the stator frame will deform and cause relatively large loads on the foundation and stator. The size of the radial load and torque must be calculated individually for each unit as there are major differences in the designs and sizes of the units.

As the sizes of the units increased, the thermal expansion became an ever-growing problem. This problem was resolved by modifying the feet of the stators so that they were free to slide radially on the foundation. In this type of design, the stator foot stands on the foundation and is guided radially by a wedge which allows the stator foot to slide radially but prevents it moving tangentially. Ideally, the radial load and the torque over the foot due to thermal expansion would be eliminated entirely in this way. However, it has been found that a large number of sliding stator feet lock due to misalignment of the wedges and because the stator foot and foundation are not parallel, and also due to an uneven vertical load between the stator feet. These faults introduce forces in the foundations which are difficult to estimate and for which they are not normally designed.

Over the past decade fixed feet have become more common again, but with flexible stator pillars. The stator frames have been provided with flexible pillars in order to minimize the thermal load on the foundation and stator. This means that the stator foot is located on a pillar which in turn is connected to the stator.

The function of these pillars, as well as carrying the weight of the stator and absorbing the torque, is to allow thermal expansion of the stator. The stator's radial change due to a change in temperature means that the pillars will bend, to reduce the load on the unit and foundation. However, the disadvantage of the pillar is that the stiffness in the stator will be reduced in both the radial and the tangential direction, which means that movements will be larger in the event of short circuit or magnetic unbalance, for example. The advantage is that the stator has a defined position which will not change over time due to the fact that the feet move uniformly in relation to the foundation.

2.1.4 Fault cases

Electrical faults in the generator which affect the surrounding structure are primarily different types of short circuits. Short circuits in the generator may be three-phase short circuits, two-phase short circuits, short circuits between phase and earth, and a semi-shorted rotor. The three or two-phase short circuits normally have the greatest impact on the surrounding structure. The size of the loads acting on the foundation is dependent on the size of the short circuit moment in the air gap, the stator's stiffness and mass moment of inertia.

A short circuit in the generator will affect the surrounding structure with a number of load cycles and with a high load level before the unit's protection disconnects the unit. The loads arising in the event of a short circuit are dependent on the type of short circuit and how the unit is designed. To reduce the load on the unit and foundation in the event of a short circuit, the stiffness of the stator shall be designed so that the stator's natural frequency does not coincide with the short circuit frequency.

The short circuit moment in the air gap is in many cases in the order of five to fifteen times greater than the unit's nominal torque and oscillates at the net frequency and multiples of the net frequency. Figure 2—5 presents an example of torques in the event of a short circuit for a unit where the stiffness properties of the stator have been varied so that the stator's natural frequency has been changed to f=37.4 Hz, f=21.6 Hz and f=17.6 Hz. The torque curves have been normalized with the unit's nominal torque, and in the simulations such as the curves in Figure 2—5 the maximum value of the short circuit moment in the air gap is eight times as great as the nominal torque.

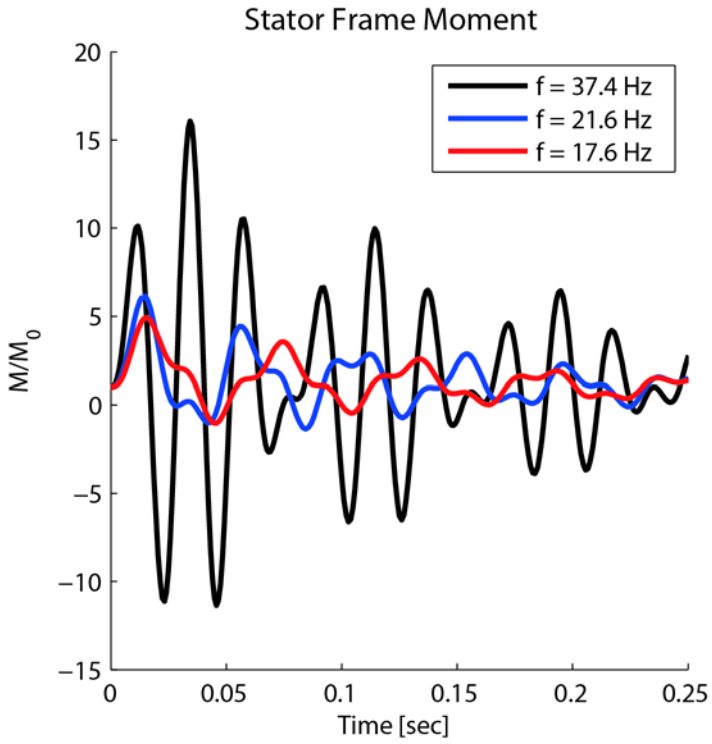

Figure 2—5: Torque acting on the stator when a short circuit occurs.

The short circuit moment gives rise to a torque at the stator which will affect the foundation with loads. The size of the foundation loads is dependent upon the stator's moment of inertia and stiffness in the torsion direction and the radius of the stator's foundation. This means that the load from a short circuit must be analyzed separately for each unit, which is normally done by the suppliers of the generators: the results are then reported to the unit owner.

2.2 Turbines

Hydroelectric power systems became common in the early 20th century. Many of the early hydropower units had horizontal Francis turbines. Vertical machines became more common towards the mid-20th century, and in 1926 the world's first "large" hydropower unit with a Kaplan turbine was commissioned. This was the Lilla Edet turbine with a runner diameter of 5.8 m and a rated power of 8 MW.

The introduction stated that loads from turbines of Kaplan and Francis types would be discussed in this report. Figure 2—6 shows what these turbines look like. For a turbine of Kaplan type, the angles of the guide vane and runner blade are adapted on the basis of the prevailing pressure and flow conditions, as well as the required power output. For the Francis turbine, the water flow is controlled solely using the guide vanes.

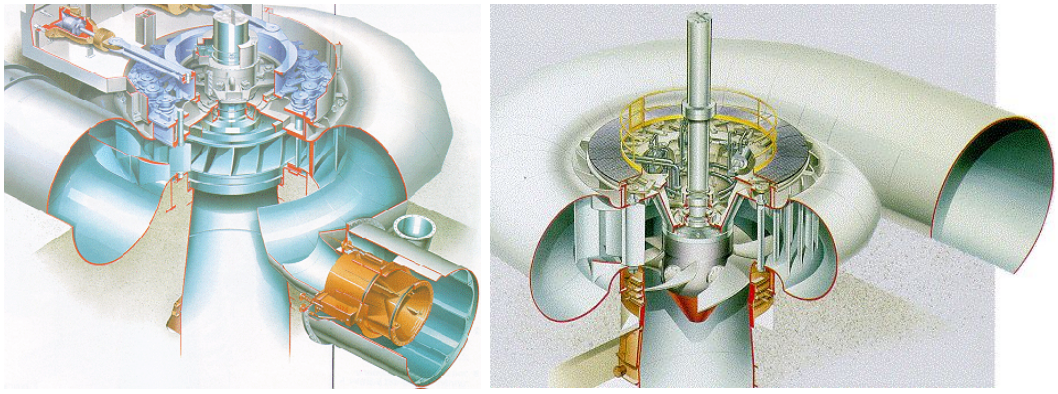

Figure 2—6: Francis and Kaplan runner (www.tfd.chalmers.se).

The loads occurring at the runner are mechanical and hydraulic loads, and these loads have both a static and a dynamic impact on the surrounding structure.

2.2.1 Mechanical loads

The mechanical loads which the runner gives rise to are axial load from its own weight and radial loads caused by mechanical unbalance. Runners are generally balanced by a "static" balancing on the workshop floor, and the permitted residual unbalance is determining on the basis of the ISO-1940 standard. Speed, permissible residual specific unbalance value, eccentricity on assembly of runners and the turbine shaft's radial displacement in the guide bearing determines the radial mechanical loads occurring at the runner.

2.2.2 Hydraulic loads

When the water passes the runner, an axial hydraulic load occurs which is also absorbed by the thrust bearing and its supporting structure. This hydraulic load is dependent upon the unit's operating mode. The Kaplan turbine is a reaction turbine, which means that it is possible to estimate static axial load during stationary operation on the basis of the pressure drop over the runner and its area. The Francis turbine is a mixture of an impulse turbine and a reaction turbine, which means that it is not as easy to estimate axial loads. When replacing runner or constructing new units, the turbine manufacturers identify the static axial loads by means of model tests or numeric calculations. It is also possible to determine the axial load on existing units by measuring axial strain in the turbine shaft. Figure 2—7 shows results from axial load measurements from a 42 MW Kaplan turbine operating during load ramp (i.e. non-stationary operation).

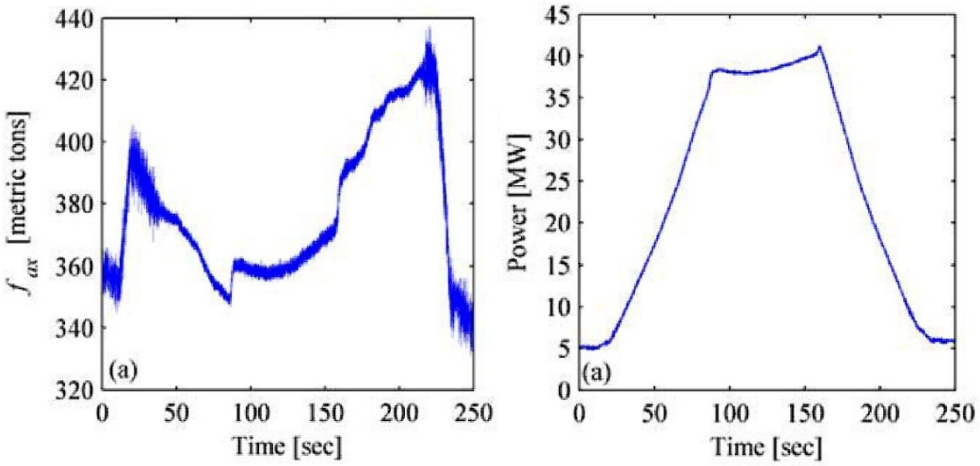

Figure 2—7: Axial load from hydraulic load and power output (42 MW Kaplan).

The radial and axial loads occurring at the runner are both static and dynamic. The amplitude and frequency of these loads are dependent upon the turbine type and operating mode. The radial load is mostly absorbed by the turbine guide bearing and its supporting structure. In some operating modes, periodic disruptions from the waterway may cause static and dynamic loads with high amplitude.

Figure 2—8 shows the measured load at idle and 70% load for a 42 MW Kaplan. As regards the determination of loads at runners (static and dynamic plus axial and radial), there are currently no clear guidelines regarding prevailing load levels. However, work is ongoing among both suppliers and power plant owners as regards identification of these loads, which will probably help to make this clearer in the future.

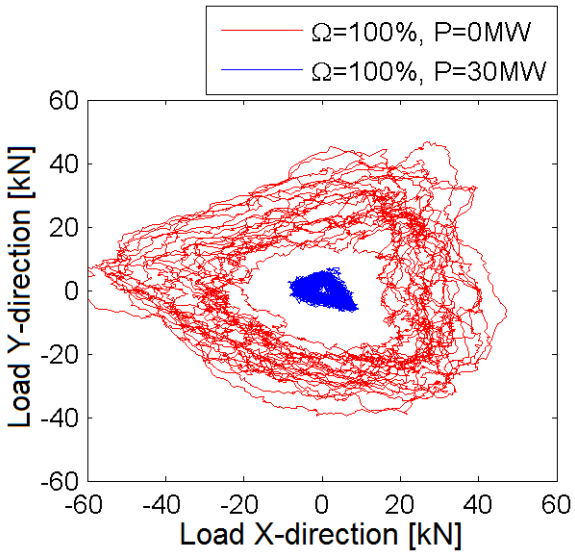

Figure 2—8: Measured radial load at the turbine guide bearing at 0 and 70% power.

For runners of Francis type, pressure may in some instances occur between the runner's top side and the underside of the turbine cover, which can cause increased axial load.

2.2.3 Fault cases

Fault cases which may occur and which have a major impact on the loads for the concrete structure are load rejection, emergency stop, runaway and uncontrolled closing of guide vanes. Furthermore, mechanical faults such as linkage rupture and blade rupture results in high loads on surrounding structure.

Load rejection/emergency stop take place when a fault occurs in the system and the braking torque from the generator is deactivated. This result in a speed increase in the unit and in some cases causes adverse flow conditions at the runner and natural frequencies may be excited. Figure 2—9 shows an example of a case of this type, and it is clear from measured displacements in the turbine guide bearing that the radial forces increase markedly in this fault case.

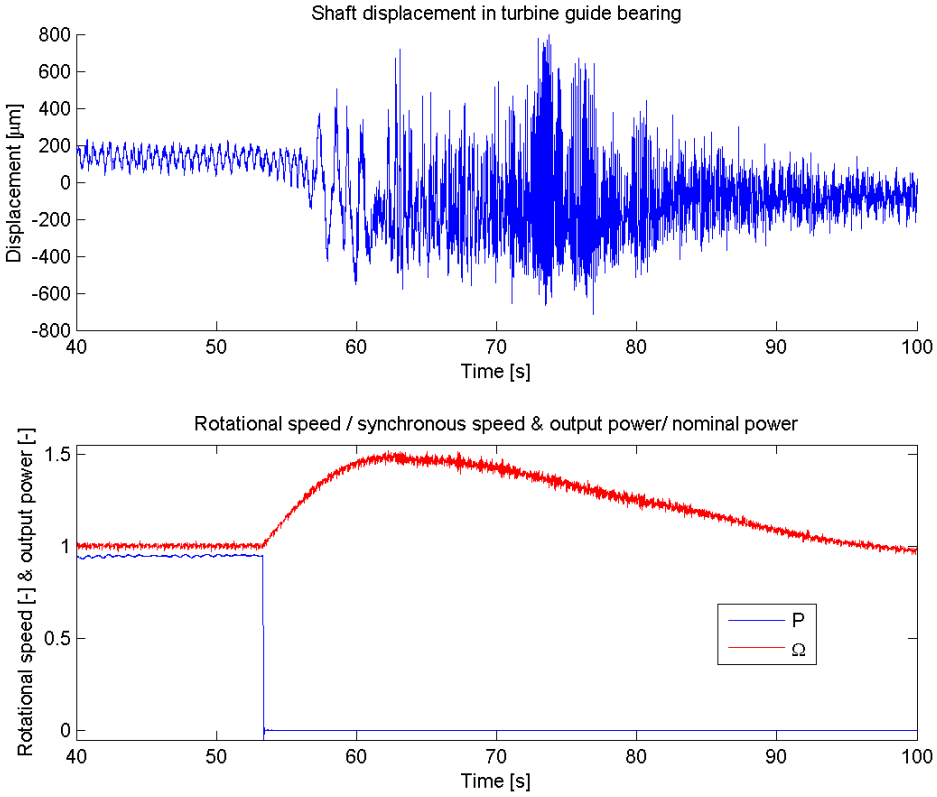

Figure 2—9: Measured radial shaft displacement at emergency stop at maximum power (large Kaplan unit).

Off-cam runaway means that the regulation of the guide vanes and runner blades is disabled and stuck in open position. This means that the runner rotates in non-optimal flow conditions and that the force from mechanical unbalance increases markedly due to the increased speed.

Water hammer due to uncontrolled closing of guide vanes has occurred in the case of a few units, with costly consequences (Hillgren, 2011). Uncontrolled closing of guide vanes occurs when the design elements which regulate the guide vanes are designed incorrectly and permit fast closing of several or all guide vanes. This may result in creation of a vacuum under the runner, and when the water then comes back water hammer occurs. This results in high axial forces on the runner and turbine cover.

2.3 Supporting structure

In this report, the supporting structure is defined as the structure sited between the rotating system and the concrete structure. The loads which occur in the rotating system are propagated via the supporting structure and out to the concrete structure. Besides the loads from the rotating system, the supporting structure's own weight, its thermal expansion and any excitations of the supporting structure's natural frequencies contribute to the loads which act on the concrete structure.

2.3.1 Load distribution, supporting structure

In the case of a unit with two guide bearings, one turbine bearing and one bearing above or below the generator, the load distribution between the bearings can be determined easily as the system is determined statically. For units with three bearings, the load distribution between the bearings is slightly more complex as the system requires attention to be paid to stiffness in the shaft, bearings and bearing brackets in order to achieve the correct load distribution across the supports. The generator bearings are often located relatively close to the generator rotor, which means that the generator rotor's unbalance force is distributed between the generator bearings and the turbine's unbalance force is mostly absorbed by the turbine bearing.

2.3.2 Design, supporting structure

Bearing brackets are used at the upper and lower generator guide bearings to hold the shaft in position and propagate radial forces or a combination of radial and axial forces to the concrete structure. Bearing brackets' ability to transfer force to the concrete structure is dependent upon its design. Figures 2—10 to 2—12 show a number of common design solutions relating to bearing brackets surrounding the generator bearings. The bearing brackets are subject to temperature variations due to the generator heating up nearby structure when it is operational. This means that the supporting structure's thermal expansion affects the loads which are transferred to the concrete structure.

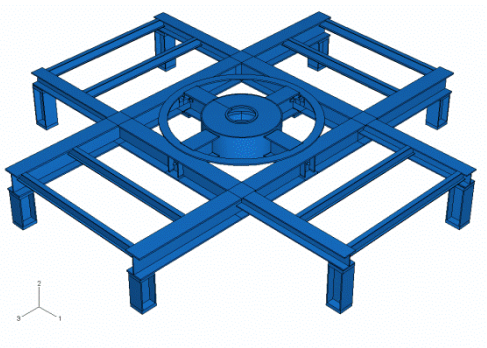

Figure 2—10: Medium-sized units, “H-bracket” above generator.

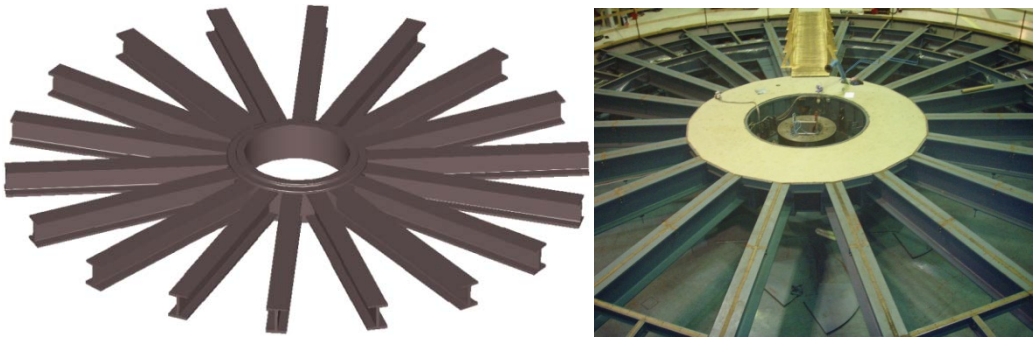

Figure 2—11: Large units, “spoke wheel” bracket above generator.

The bearing brackets shown in Figures 2—10 and 2—11 are examples of bearing brackets positioned above the generator. Great temperature variations occur above the generator depending on whether the unit is operational or shut down, which means thermal expansion and contraction in the bearing brackets. These bearing brackets are generally made up of large beams with I or H cross sections, and the loads will be transmitted to the concrete structure depending on their attachment to the concrete structure. Bearing brackets of the type shown in Figure 2—10 (“H–brackets”) rest on the supporting structure for the stators, and in some cases this type of bearing bracket is not connected to the surrounding concrete structure.

Figure 2—12 shows the appearance of a common bearing bracket, positioned beneath the generator, in a hydropower unit manufactured between 1950 and 1970. These absorb loads from the generator guide bearing beneath the generator and the journal bearing. The bearing bracket is subjected to both axial and radial forces there, and this design is also subject to major temperature variations depending on whether the unit is operational or shut down. Figure 2—13 shows an example of a bearing bracket positioned near the runner.

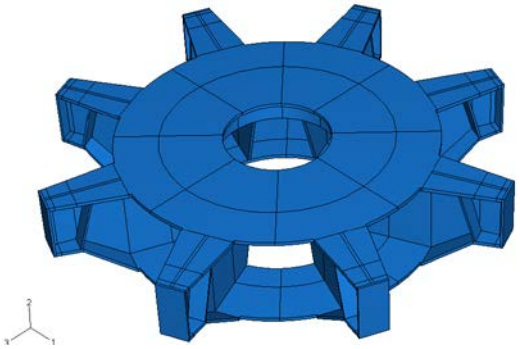

Figure 2—12: Bearing bracket for axial and radial force positioned beneath the generator.

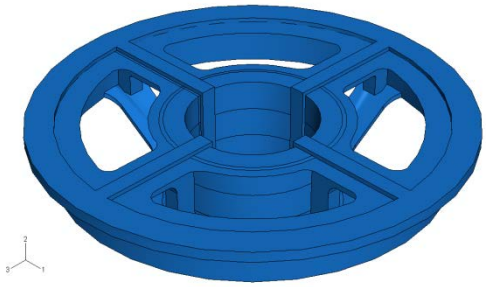

Figure 2—13: Bearing bracket, turbine guide bearings.

The brake system in the hydropower unit may also result in axial and tangential load cycles on the supporting structure during starting and stopping. Most large hydropower units are designed to have the braking track fitted on the underside of the rotor ring, which means that the static part of the brake system is fitted to the supporting structure/concrete structure beneath the rotor.

The temperature is relatively constant at the supporting structure which surrounds the turbine guide bearing, which means that no major geometric changes occur in this supporting structure due to temperature changes. For units with Kaplan turbines, the turbine guide bearing is often connected to a bearing bracket which is attached to the turbine cover: see Figure 3—1. Another common design solution is for the turbine guide bearing to be connected directly to the turbine cover. The turbine cover there absorbs radial loads coming from the turbine guide bearing, as well as any axial loads occurring above the runner.

3 Loads at interconnection between supporting structure and concrete

Loads described in the previous section will be transferred to the concrete structure in one way or another. Earlier sections in this report indicate that combinations of loads from several machine components act on the concrete foundations.

Figure 3—1 show a cross-section of a hydropower unit, and the red squares are interconnections where the loads from the unit are transferred to the concrete structure. Depending on the design of the hydropower unit, these interconnections may be in different locations and designed in different ways. The loads occurring between rotor and stator will be absorbed at the point where the stator is attached to the concrete, and to keep the system in equilibrium the loads on the rotor are absorbed by the bearing brackets' attachments over or/and under the generator.

Hydropower units are all individuals, and the load levels occurring in a unit are dependent on its design, how maintenance has been carried out (e.g. balancing or alignment of stator feet) and the operating conditions to which the unit has been subject. To carry out a good estimate of the loads which act on the concrete structure, there should be an FE-model of the unit, an awareness of shaped deviations in the generator, balancing, etc. The sections below show examples of attachments between the supporting structure and concrete and procedures for estimating the loads which act on the concrete structure.

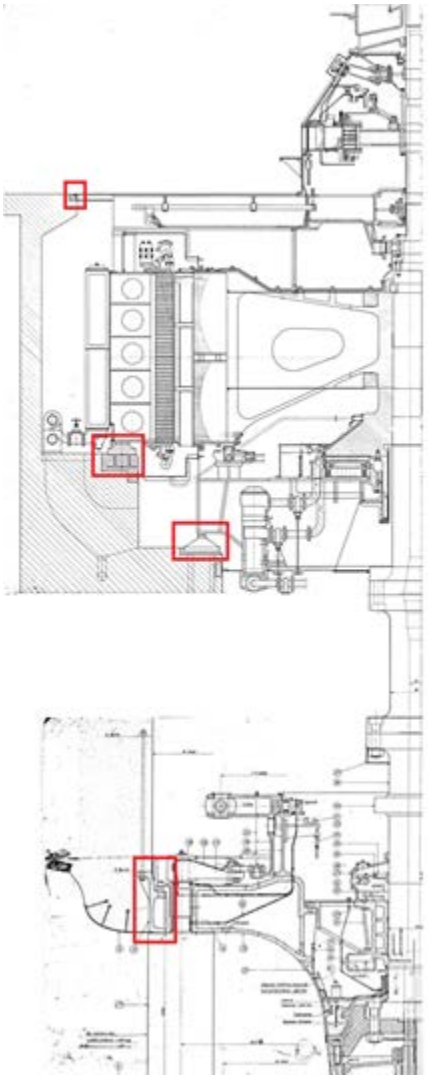

Figure 3—1: Overview of interconnections between support structure and concrete structure.

Attachment to concrete is designed in different ways depending on the design of the supporting structure and the type of loads for which the supporting structure is designed to absorb.

3.1 Radial loads

Figure 3—2 shows pictures of the interconnections to the concrete structure for two different bearing brackets mounted above a generator. The picture on the left describes the interconnection of an “H-bracket”. This bearing bracket is attached at both the stator frame and the surrounding concrete structure, and this is the same structure shown as the upper bearing bracket in Figure 3—1. This means that parts of the radial load will be passed by the bearing bracket's interconnection to the concrete and that parts of the radial load will be passed down into the stator frame. There are also structural solutions which are designed to allow the entire load from the bearing bracket to pass down into the stator frame, which means that the upper bearing bracket has no attachment in the concrete structure or simply has support for the floorboards to the concrete structure.

Figure 3—2: Interconnection of the “H-bracket” (left) and interconnection of the “spoke wheel” bracket (right).

The picture on the right in Figure 3—2 shows the attachment of an upper bearing bracket of a type installed in most of the large hydropower units in Sweden. The bearing bracket's interconnection to the concrete structure is pre-tensioned against the concrete structure by means of a screw and a number of disc springs. The stiffness of the disc springs determines the loads which the thermal expansion of the bearing bracket will give rise to. Static and dynamic loads from the rotating system will also be transferred through the bearing bracket's interconnection in to the concrete structure. The bearing bracket of the type shown in the picture on the right in Figure 3—2 rests on the stator frame, but the supports are designed so that they permit radial sliding. This means that the loads which pass down in the stator frame shall be small in relation to the loads which pass out in the interconnection to the concrete structure.

3.1.1 Properties of radial loads which act on the interconnection between the supporting structure and concrete structure

If there only is one bearing bracket which supports the generator shaft, all radial load from the generator will act on this bearing bracket, but if there is both an upper and a lower bearing bracket the loads will be distributed between the bearing brackets.

Mechanical radial forces: The mechanical forces which act on the foundation at the upper bearing bracket are caused by mechanical unbalances. The prevailing residual unbalance determines how high these loads are. For rotating components in a hydropower unit, ISO-1940 recommends a balancing degree of G6.3. This means that the mechanical unbalance force from the rotor is determined using Equation 4.

$$f_m = m_r \mathrm{e}_r \Omega^2 \tag{4}$$

where $e_r\Omega$ is 6.3/1000 [m·rad/s], m_r is the mass of the rotor and Ω is the unit's synchronous angular velocity.

Electrical forces: Forces on the foundation caused by electrical forces are caused by form defects and eccentricities in the generator. Stator eccentricity causes static loads which act on the foundations. Rotor eccentricity and form defects in the rotor and stator cause dynamic loads on the foundations. The generator's eccentricities and form defects are determined by measuring the air gap during operation. Permitted levels of form defects and eccentricities are specified by the power plant owner, and in most instances are just a few percent of the nominal air gap. The radial force which these form defects give rise to can be determined using Equation 3 in section 2.1.2. For existing power plants, the linearized magnetic stiffness, k_G, is often presented in the generator drawing, and in this instance the radial force can be determined using Equation 5.

$$f_G = e\,k_G \tag{5}$$

Thermal loads: The bearing bracket expands when the temperature of the generator increases. For most units, the beams of the bearing brackets are stiff in relation to the interconnection to the stator frame, as well as its interconnection between the bearing bracket and the concrete structure. The force which the expansion gives rise to is determined by the linear expansion multiplied by the stiffness of the interconnection.

The stiffness relationship between the bearing bracket's interconnection to the concrete structure and the bearing bracket's interconnection to the stator determines how much of the mechanical and electrical forces act on the concrete structure.

3.2 Combined radial and axial loads

Figure 3—3 shows an interconnection between the concrete structure and the bearing bracket which surrounds a combined thrust and guide bearing. The loads which act on this interconnection are radial forces from the rotating system and thermal expansion of the bearing bracket. The axial load supported by the thrust bearing must also be absorbed by the foundations.

For the interconnection shown in Figure 3—3, there is a locating pin between the bearing bracket and the foundation. In combination with the fact that there is a "gap" between the axial screw and the hole which secures the bearing bracket in the foundation, this allow the bearing bracket's thermal expansion to take place with low loads being transferred down into the foundation. The design solutions for these interconnections between the bearing bracket and the foundation vary between the units, which mean that the loads which act on these interconnections also vary between the units. However, experience has shown that in several instances, cracks have occurred between in the concrete foundation near the supports (Malm et al., 2013).

Figure 3—3: Interconnection of the bearing bracket below the generator subject to axial and radial loads.

3.2.1 Properties of combined loads which act on the interconnection between the supporting structure and concrete structure

If there is only one bearing bracket which supports the generator shaft, all radial load from the generator will act on this bearing bracket, but if there is both an upper and a lower bearing bracket the loads will be distributed between the bearing brackets.

Mechanical and electrical forces from the rotating system are the same as for the supporting structure in section 3.1.1. As far as thermal loads are concerned, the types of bearing bracket shown in Figure 2—12 are large as these also withstand the axial load from the rotating system. The force which this expansion gives rise to in this case also is dependent on the expansion amplitude and the properties of the interconnection. The forces this expansion gives rise to are dependent on the stiffness/friction properties of the interconnection to the concrete. The design in Figure 3—3 is a friction joint, which means the interconnection between the bearing bracket and the foundation starts to slide only when the radial loads have exceeded the "friction force". Loads from the unit's own weight and hydraulic loads also act on this surface. Any sliding in the tangential direction within this connection is on the other hand restricted, as discussed earlier.

In some cases the tangential forces arising from the unit's brake system is propagated through the interconnection shown in Figure 3—3.

3.3 The generator's interconnection in the concrete structure

Figure 3—4 shows pictures of three different generator foundations, sliding feet on the left, a "bolted" stator on the middle and a pillar on the right. The function of these is to keep the stator centered and free of shape deviations by managing the radial, axial and tangential forces arising in the stator. The loads which act on the concrete structure are clearly linked to the design of the interconnection. The electrical and mechanical loads which act on the upper and lower bearing brackets will also act on the generator's foundation in the opposite direction/phase. Besides these forces, tangential forces act on the foundation arising from the torque ($M_v = P/\omega$) occurring in the air gap between the rotor and the stator, axial forces from the stator's own weight and radial forces from the stator's thermal expansion. The unit's power output is denoted as P and the angular velocity as ω (rad/s).

Figure 3—4: Interconnection of a stator with sliding feet (left), a bolted stator (center) and a stator with a pillar under construction (right).

The forces the thermal expansion gives rise to are dependent on the stiffness/function of the interconnection between the stator and the concrete structure. For stators with pillars and bolted stators, the stator's thermal expansion and its stiffness can be determined on the basis of FE calculations. For units with sliding feet, these forces are harder to identify as these forces must be relatively low when the feet work as they should, but experience has shown that in reality, high loads occur at this type of supports.

One important load case to observe when designing a generator foundation is short circuit. High tangential forces occur in the event of a short circuit, and these forces are determined on the basis of the short circuit torque occurring between the stator and the rotor, as well as the design of the stator: see Figure 2—5.

3.4 The turbine covers interconnection in the concrete structure

It was stated in earlier sections that radial loads from the runner and any axial loads from pressure on the top of the runner act on the turbine cover and its interconnection to the concrete structure. Drawings of the turbine cover and connections to the concrete structure are shown in Figure 3—5.

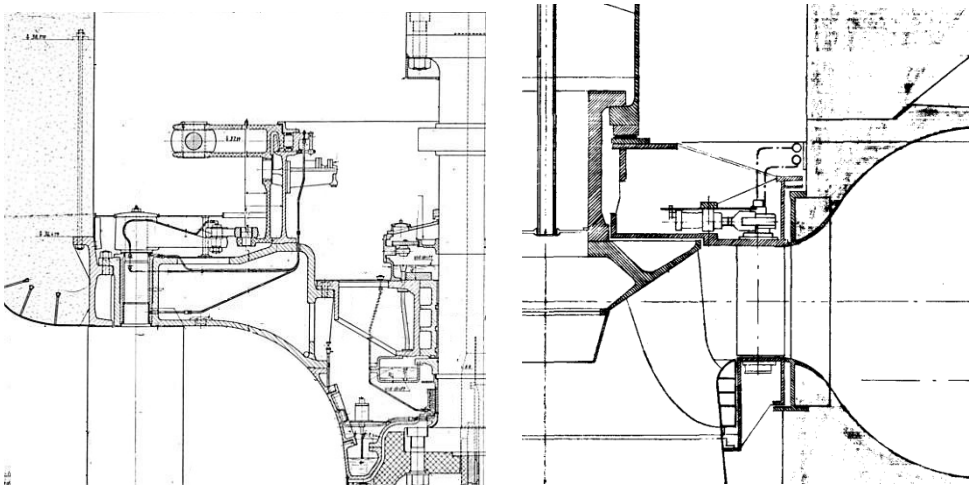

Figure 3—5: Drawings describing the interconnection between the turbine cover and the concrete structure.

Mechanical loads: The mechanical forces which act on the interconnection at the turbine cover are caused by the balancing of the runner and the runner's eccentricity on installation of the turbine shaft. As far as balancing is concerned, the balancing degree G6.3 for runners as stated in ISO 1940 is also recommended. Unbalanced forces are determined in the same way as for the generator, see section 3.1.1.

Hydraulic loads: As far as radial loads at the runner are concerned, the mechanical loads are generally low in relation to the hydraulic loads. Unfortunately, there are no clear approximate methods to determine hydraulic radial loads in hydropower units. The few measurements published show that the radial forces which the runner gives rise to in normal operating modes are between 10 and 100 kN (Nässelqvist et al., 2012).

4 Finite element model

The objective of this study is to understand the complex interaction between the power generating system (stator, rotor, turbine, etc.) and the supporting concrete structure, which is needed for formulation of more realistic and accurate specifications regarding load, stiffness and displacement levels and tolerances. The achievement of the objective requires models that account for the behaviour of the mechanical systems, supporting structures, concrete foundation and their interaction under various loading conditions. The various loading conditions include the mechanical loads (static, dynamic, short-term, long-term, etc.) such as weight of the structures and systems, and operating loads caused by the turbine, rotor, stator, etc.

The work presented here is limited to the modelling of the behaviour of the foundation under the influence of the dead weight, and the interaction of the foundation with the stator and rotor spider.

4.1 Object specific data for analysed hydro power plant

The rotor dynamic model is based on the design of generators no. 14 and 15 located at the Hojum hydro power plant. This generator design uses three radial bearings, i.e. upper and lower rotor bearings, and a turbine bearing. The vertical load from the shaft is supported by an axial bearing located at the lower rotor guide bearing bracket. These units have a power rating of 47 MW and an operational rotational speed of 136.4 RPM. The complex geometries for the generator bearing brackets are simplified for the simulations to obtain a simplified model, with the use of radial springs to model the dominating behaviour of these brackets. Furthermore, the bearings properties are also simplified for the model and only consider stiffness and damping in radial direction. A typical rotation speed for hydro power generators equal to 150 RPM is used for the structural interaction analyses.

Initially the rotating system is well balanced according to earlier discussions in section 2.1.1. However, older generators may be subjected to greater unbalanced forces. The unbalanced force for these simulations was therefore increased to twice the recommended value G6.3. Furthermore, the requirement regarding the balancing is for components and tolerances for the assembly of the generator add to the unbalanced force.

This study doesn't consider exceptional loading due to e.g. water hammer or short circuit. The modelling of these highly dynamic events would require a considerable increase in the complexity for the modelling of the mechanical components, i.e. the bearing brackets and the support structure for the stator. The properties of these components are likely to strongly influence the magnitude of the dynamic forces acting on the concrete foundation during exceptional loading conditions.

4.2 Dynamic FE analysis of rotor for hydro power unit

A 3D rotor dynamic FE model is developed in Abaqus version 6.11. The aim for this initial part of the study is to verify the dynamic properties for the Abaqus FE model for analyses of hydro power units. An independent rotor dynamic analysis of the system, combined with data regarding the stiffness for the spiders and bearings, is used for reference. The reason for this is to obtain comparable simulation results, and thereby identify any major discrepancies between the responses for the two analyses.

The geometry and properties for the Abaqus model are based on a rotor dynamic analysis performed with RAPPID version 3.00 from Rotordynamics-Seal Research, Loomis, California. However, the data used for the RAPPID analyses needs to be matched to the Abaqus FE model. One limitation for Abaqus, and likely other general FE codes, is that nodes with prescribed rotational inertia can't be located at the axis of revolution for the shaft, since the rotational angle can't be defined for a node located at the distance zero from the rotational axis of the shaft. Therefore, the rotational inertia given at discrete points are approximated with physical bodies instead and node locations needs to be given consequently with this, resulting in minor errors for the polar and diametral moments of inertia e.g. for the rotor. This also applies for the turbine, guide bearings and exciter. The modelling concept is verified by frequency analyses of the shaft and comparison with the RAPPID.

4.2.1 Geometry and material properties

The shaft and rotating masses representing rotor, turbine and bearings are modelled with 3D beam elements. The element type for the shaft is two node beam elements with constant cross section designated as B31 in Abaqus. The cross sections for the shaft are given in Table 4—1 below. Elements no. 17 to 19 are slightly tapered on the outside for the frequency analysis performed with RAPPID, with the outer diameter at the top of the element given in the table. Furthermore, elements no. 33 and 34 are tapered on the inside for the RAPPID analysis. The original geometry for the shaft and the simplified geometry used for the Abaqus analyses are both shown in Figure 4—1. All analyses also include a 0.68 m high hollow cylinder located at a distance of 2.595 m to 3.275 m from the top, with an outer diameter of 1.24 m and its inner diameter given by the shaft diameter. This cylinder has the same density as the shaft, but with neglectable stiffness and only adds inertia to the FE model. Furthermore, locally added rotation inertia for the two models are given in Table 4—2.

Table 4—1: Shaft diameter and beam element lengths, see also Figure 4—1.

Distance from top (m)	Element length (m)	Outer diameter (m)	Inner diameter (m)	Element no.
0.0000	0.0110	0.4100	0.320	1
0.0110	0.1240	0.4450	0.320	2
0.1350	0.4250	0.4500	0.320	3
0.5600	0.1000	0.5500	0.320	4
0.6600	0.1000	0.5500	0.320	5
0.7600	0.0400	0.5500	0.320	6
0.8000	0.1000	0.5460	0.320	7
0.9000	0.3100	0.5495	0.320	8
1.2100	0.1500	0.4900	0.320	9
1.3600	0.1500	0.5520	0.320	10
1.5100	0.2200	0.5550	0.320	11
1.7300	0.1050	0.5800	0.320	12
1.8350	0.1400	0.5800	0.320	13
1.9750	0.1515	0.5950	0.320	14
2.1265	0.1810	0.6000	0.320	15
2.3075	0.2875	0.6100	0.320	16
2.5950	0.1295	0.6100	0.320	17*
2.7245	0.1800	0.7220	0.320	18*
2.9045	0.1705	0.8000	0.320	19*
3.0750	0.1000	0.7900	0.320	20
3.1750	0.1000	0.7900	0.320	21
3.2750	0.7000	0.7900	0.320	22
3.9750	0.5000	0.8000	0.320	23
4.4750	0.1000	0.8000	0.320	24
4.5750	0.3550	0.8050	0.320	25
4.9300	0.2250	0.8100	0.320	26
5.1550	0.0712	0.8100	0.320	27
5.2262	0.0458	0.8100	0.320	28
5.2720	0.0300	0.8200	0.320	29
5.3020	0.7240	0.8000	0.320	30
6.0260	0.7240	0.8000	0.320	31
6.7500	0.7250	0.8000	0.320	32
7.4750	0.3100	0.8000	0.320	33*
7.7850	0.2200	1.4500	0.408	34*
8.0050	0.2200	1.4500	0.150	35
8.2250	1.2950	0.8200	0.150	36
9.5200	1.2950	0.8200	0.150	37
10.8150	1.2950	0.8200	0.150	38
12.1100	0.1500	1.0000	0.150	39
12.2600	0.0500	0.8200	0.150	40
12.3100	0.5950	0.8200	0.150	41
12.9050	0.5950	0.8200	0.150	42
13.5000	0.2250	1.6000	0.150	43
13.7250	1.1060	1.6000	1.000	44**

Note: * Elements no. 17, 18, 19, 33 and 34 are tapered for the RAPPID frequency analysis. **: Element no. 44 has a reduced density equal to 100 kg/m^3.

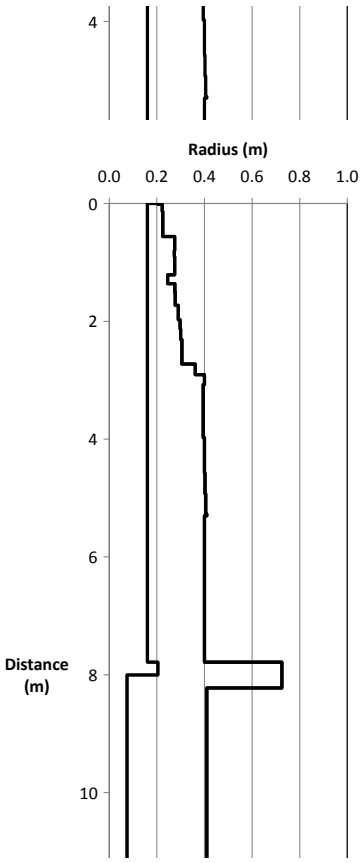

Figure 4—1: Cross section of rotor shaft model, with figure a) showing the original model for RAPPID analysis and figure b) showing the simplified geometry for Abaqus analyses.

Table 4—2: Added rotational inertia and mass.

Mass	RAPPID analysis			Abaqus analysis		
(kg)	Distance from top (m)	Polar inertia (kg-m²)	Diametral inertia (kg-m²)	Distance from top (m)	Polar inertia (kg-m²)	Diametral inertia (kg-m²)
4600	0.7600	2730	1434	0.7600	2795	1400
119800	3.1750	857125	478208	3.1750	903298	452048
119800	4.4750	857125	478208	4.4750	903298	452048
13840	5.2262	7512	4944	5.2262	8526	4273
65500	14.8310	102000	79700	14.7810	124382	62246

The material properties for the shaft are given in Table 4—3 below. However, a reduced density equal to 100 kg/m³ is used for the 1.106 m at the end of the shaft, with retained elastic properties of the material.

Table 4—3: Steel properties for shaft.

Steel	
Density	7850 kg/m^3
Young's modulus	206 GPa
Poisson's ratio	0.30

4.3 Coupled FE analysis for structure interaction analysis

A 3D solid FE model of the reinforced concrete foundation for a hydro power unit was earlier developed for Abaqus, and used for the analysis of drying diffusion, thermal and mechanical loads (Malm et al., 2013). This FE model is used as a basis for the current FE analyses. These analyses are performed with Abaqus version 6.12, and consider the coupled structural interaction between the generator and the concrete foundation. The purpose of this FE model is to simulate the response of the foundation subjected to the mechanical loads from the generator. The structural behaviour of the foundation has been analysed taking into account the dead loads and the operational loads imposed to the foundation from the rotating system and stator.

4.3.1 Geometry

The same geometry for the foundation as the earlier analysis presented by Malm et al. (2013) is used for these FE analyses. The geometry of the generator foundation is partly axisymmetric; however, there exist a few penetrations, i.e. entries and doors, in the wall of the foundation. The cross section through the foundation at a location without penetrations is shown in Figure 4—2:.

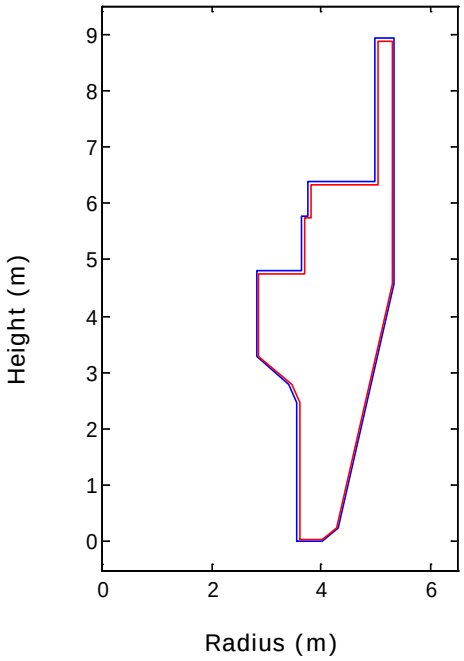

Figure 4—2: The cross section of the foundation, with the reinforcement shown in red.

Four evenly distributed penetrations are located in the upper part of the foundation, above the supports for the stator. The dimensions of these penetrations are 800x1200 mm^2 (height x width), and they are approximately placed at 0°, 90°, 180° and 270° relative to a Cartesian coordinate system placed in the centre of the foundation, see Figure 4—3. Three more penetrations can be found in the lower part of the generator foundation, also shown in Figure 4—3. One large penetration with a dimension of 2300x2000 mm^2 (height x width) is located at the angle 270°, and with a distance of 2650 mm from the centre of the penetration to the bottom of the foundation. The other two penetrations can be found at angles 0° and 180°, and their height is equal to the aforementioned penetration while the width is 1200 mm.

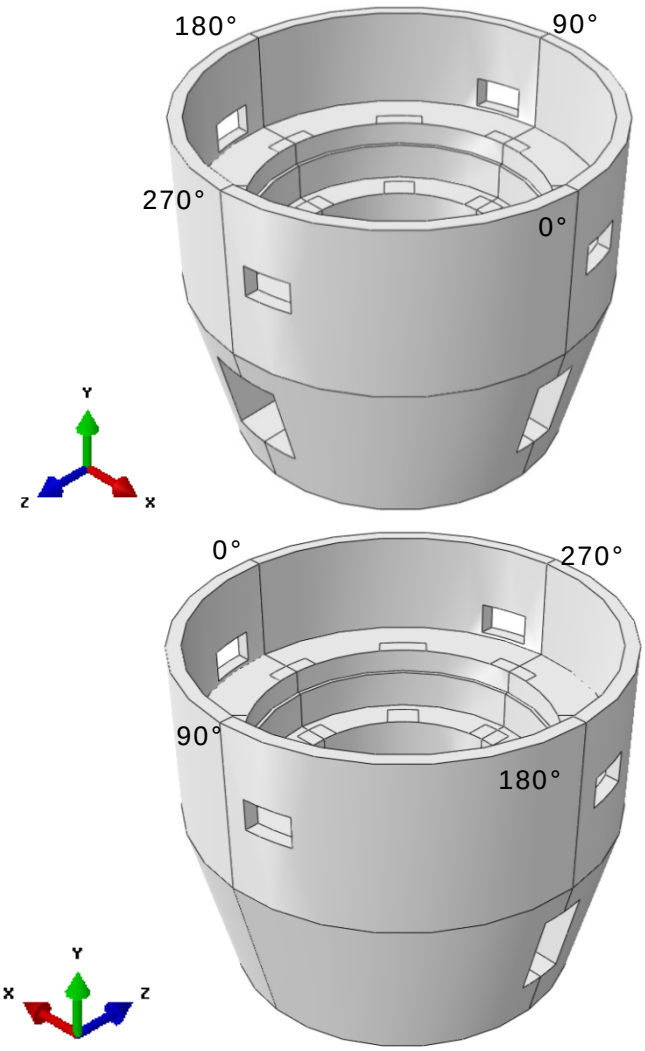

Figure 4—3: The geometry of the generator foundation from two views showing the different penetrations (Malm et al., 2013).

The reinforcement is modelled with a simplified method which assumes an evenly distributed reinforcement in two perpendicular directions (Malm et al., 2013). The average reinforcement diameter is 25 mm, with an average distance between the reinforcement bars of 250 mm. In the FE-model, the centre of the reinforcement is assumed to be placed 50 mm from the surface of the foundation; which yields a 37.5 mm concrete cover. According to the blueprints of the concrete foundation, the distance from the centre of the reinforcement to the surface should not exceed 40 mm or be less than 30 mm. These requirements are fulfilled with the assumptions made above. In Figure 4—4, the surface of the foundation is illustrated in blue and the reinforcement in red. The local geometry of the supports, e.g. location of stiffening plates and grouted bolts, is not included in the FE model.

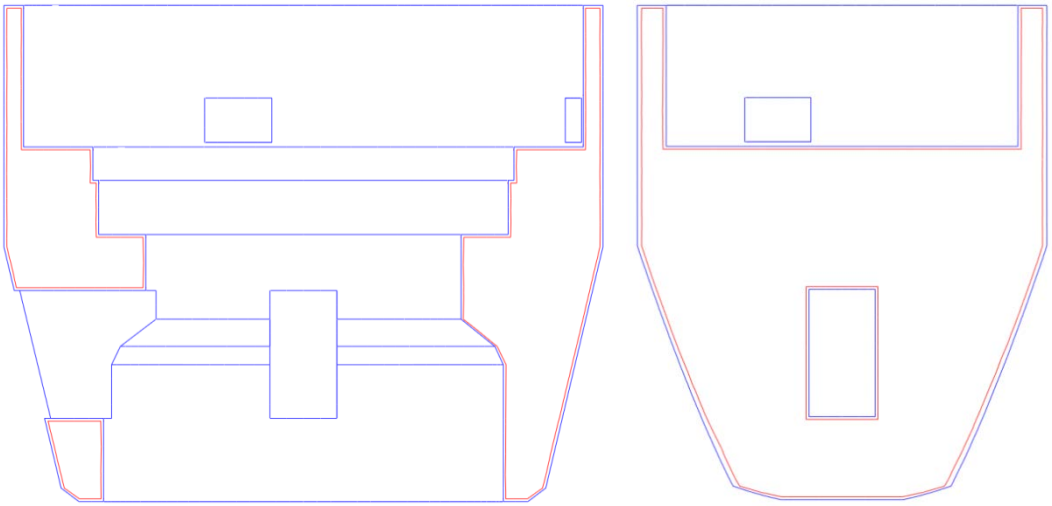

Figure 4—4: The surface of the foundation is illustrated in blue and the reinforcement in red, with two different planes through the model shown (Malm et al., 2013).

4.3.2 Mesh

A relative high mesh density is used for the analysis, compared with the mesh density used for normal structural analyses of concrete structures. This is required to be able to determine the stress field near e.g. penetrations. The element type that is used for the concrete foundation in the FE model is C3D8R, which is an 8-node hexahedron with reduced integration. Furthermore, the characteristic element size is approximate 0.2 m for the solid elements, with the FE mesh shown in Figure 4—5. The reinforcement is modelled with rebar layers defined as shell elements S4R, and the characteristic length of these elements is also approximate 0.2 m. The reinforcement is defined as embedded in the concrete, with a perfect bonding, i.e. no slip is allowed, between the reinforcement and the concrete. The model consists in total of approximate 50 000 elements and 200 000 degrees of freedom. The same mesh was used for the previous FE analyses performed by Malm et al. (2013). This mesh density is sufficient to be able to describe the crack propagation, which has been verified previously in e.g. Hassanzadeh et al. (2012). The stator and its supporting structure and cooling system are simplified as a massive hollow cylinder for the analyses, see Figure 4—6. The inner and outer diameters of the stator part are chosen as 7.52 m and 8.32 m, respectively. These dimensions are chosen to easily obtain a coupling of the stator to the earlier defined stator support areas within the foundation. Furthermore, the height of the stator part is 2.5 m. The stator part is also modelled with solid 8-node hexahedron reduced integration elements, type C3D8R, and it is connected with tied constraint to the concrete foundation at the support areas.

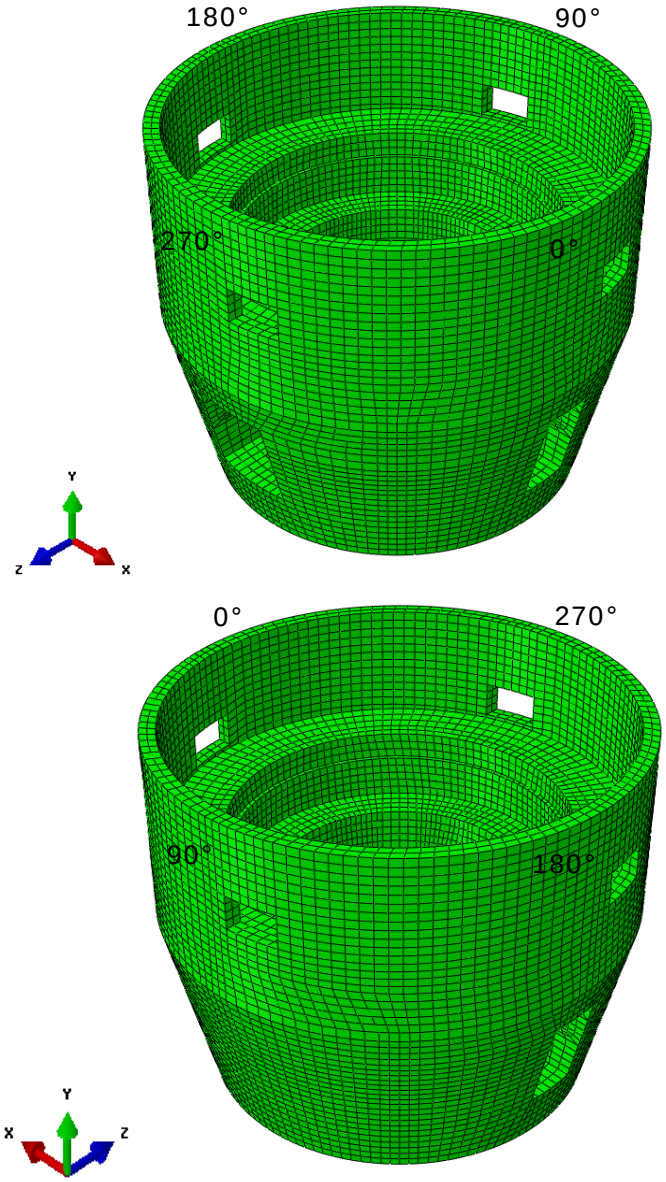

Figure 4—5: Geometric mesh of the concrete foundation (Malm et al., 2013).

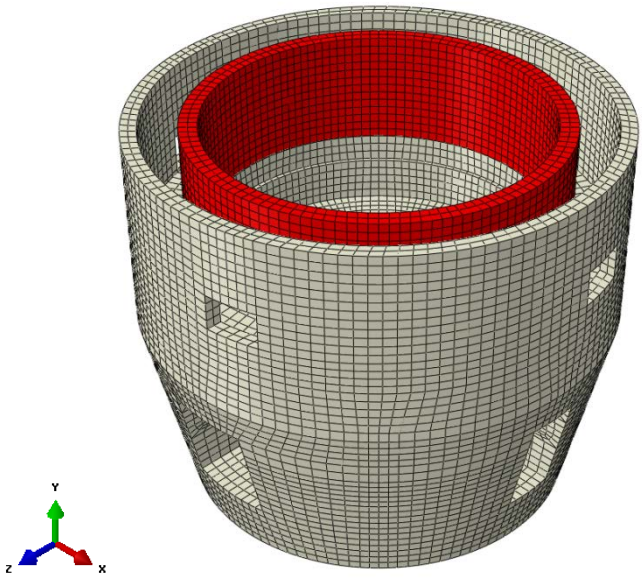

Figure 4—6: Geometric mesh of the stator and foundation.

4.3.3 Material properties

The concrete and steel material properties used in the analyses are based on the properties presented by Larsson (2010), and are given in Table 4—4 and 4—5. However, the Young's modulus for the cracked elements concrete is reduced to 0.50 GPa for the analyses that incorporate concrete cracks.

Table 4—4: Concrete material properties for un-cracked material.

Concrete	
Density	2300 kg/m^3
Young's modulus	25 GPa
Poisson's ratio	0.20

Table 4—5: Reinforcement B500 material properties.

Reinforcement	
Density	7800 kg/m^3
Young's modulus	200 GPa
Poisson's ratio	0.30

The stator and its load bearing frame are considered to be much stiffer than the upper rotor spider. Furthermore, a detailed modelling of the stator and its supporting structure would require a considerable more detailed FE model, which is beyond the scope of this study. The stator and its supporting structure are therefore modelled as a massive hollow cylinder as discussed earlier, with an equal mass to account for the dead weight acting on the stator supports. The used material data for the stator part in the model are given in Table 4—6.

Table 4—6: Stator part material properties.

Stator	
Density	5200 kg/m^3
Young's modulus	200 GPa
Poisson's ratio	0.30

4.3.4 Mechanical loads

The mechanical loads are transferred to the concrete foundation at the stator and rotor spider supports. The support areas for the rotor spider and stator are located with 45° divisions as illustrated in Figure 4—7 and have a size of 1200x400 mm^2 and 600x800 mm^2 for the stator and the rotor spider, respectively. The mechanical loads acting on the concrete foundation are summarized in Table 4—7. These loads are based on the loads presented by Larsson (2010), and were also used by Malm et al. (2013). Note that the upper generator bearing bracket is connected to the upper part of the stator in the model, i.e. the radial forces in the upper generator bearing bracket is transferred to the stator supports via the stator structure.

The vertical loads on the lower rotor spider presented in Table 4—7 are applied as uniform surface pressure on the supports for the lower generator bearing bracket, and the tangential load acting on the stator is applied as evenly distributed force on the inside of the stator. All the other loads are included within the model, incl. dead weight.

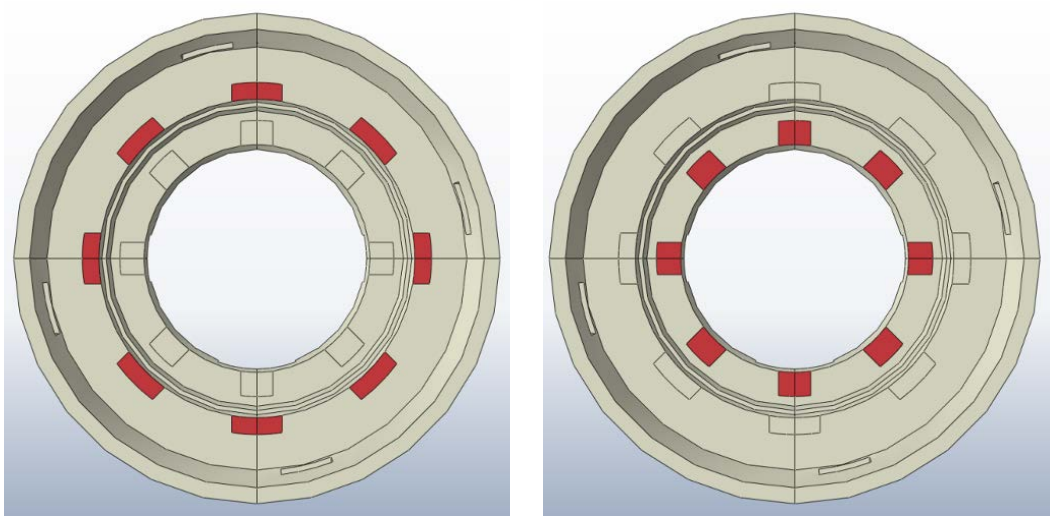

a) b)

Figure 4—7: Areas for the support for stator (a) and lower rotor spider (b), respectively.

Table 4—7: Loads caused by the power generating system.

Device	Duration	Load level
Vertical loads on stator support		
Stator	Permanent	1200 kN
Cooling system	Permanent	100 kN
	Sum	**1300 kN**
Vertical loads on the lower rotor spider (i.e. lower generator bearing bracket)		
Rotor	Permanent	2890 kN
Turbine	Permanent	1200 kN
Spider and bearing	Permanent	250 kN
Turbine cover	Permanent	530 kN
Water	Variable (normal)	5720 kN
	Sum (normal)	**10590 kN**
Tangential loads acting on the stator		
Moment acting on stator	During operation at nominal rotation speed	4974 kNm
Radial loads acting on the stator		
Load caused by magnetic eccentricity.	During operation, dynamic.	From interaction with rotating system.
Radial loads acting on the rotor spider supports		
Load caused by magnetic eccentricity.	During operation, dynamic.	From interaction with rotating system. *
Load caused by unbalanced force.	During operation, dynamic.	From interaction with rotating system. *

Note: * See section 4.3.5 for description of the structural interaction modelling.

4.3.5 Coupled generator model

The earlier described rotor dynamic model is coupled to the foundation at the lower rotor spider support areas and to the stator, with the lower and upper rotor spiders modelled with 3D spring elements. The stiffness of these radially located connector elements are selected to give approximately the same stiffness as the lower and upper rotor spiders, respectively. The radial

connector elements representing the upper rotor spider are connected to the upper surface of the stator, with the spring elements representing the lower rotor spider connected between the lower rotor bearing location and the concrete foundation. The properties of the connector elements are given in Table 4—8, with a cross section of the model shown in Figure 4—8. Furthermore, the bearing bracket located near the turbine is also modelled with radially located connector elements. However, these connector elements are connected to ground.

All radial bearings are modelled as radial connector elements with damping, with the element properties chosen to correspond to the bearing properties at a rotational velocity of 150 RPM.

The load caused by magnetic eccentricity is modelled with springs, using a negative stiffness in radial direction, connected between the shaft and the stator. The negative stiffness of these springs is chosen to give a resulting force between the shaft and stator approximately equal to the magnetic force due to eccentricity. Furthermore, this magnetic pull force can be considered linear for deformations less than 10% of the air gap for a generator. The spring stiffness for the elements are also given below in Table 4—8. For simplicity, these springs are placed with the same angular division as for the upper and lower rotor spiders, i.e. 45° divisions.

Furthermore, the mass of the bearings and bearing brackets are in the model represented by discrete masses given in Table 4—9. This is to obtain a realistic dynamic behaviour of the bearings and bearing brackets, and to be able to calculate the radial forces acting on the structure. This also applies to the bearing located near the turbine and the turbine cover. The radial forces from the turbine bearing bracket does not directly contribute to forces acting on the modelled part of concrete foundation, instead the dynamic response at the location of the turbine bearings influence the dynamic behaviour of the shaft, and indirectly the forces in the lower and upper rotor bearing brackets.

Table 4—8: Properties for connector and spring elements.

	Spring stiffness	Damping	Angular division
Upper rotor spider, radial stiffness 800 MN/m	166 MN/m	No damping	45°
Lower rotor spider, radial stiffness 2900 MN/m	601 MN/m	No damping	45°
Turbine bearing bracket, radial stiffness 3000 MN/m	621 MN/m	No damping	45°
Upper generator bearing	1825 MN/m	52.1 MNs/m	Not applicable
Lower generator bearing	862 MN/m	27.7 MNs/m	Not applicable
Turbine guide bearing	1341 MN/m	41.0 MNs/m	Not applicable
Magnetic eccentricity, 300 MN/m	-62.1 MN/m	No damping	45°

Table 4—9: Lumped node masses for spring-mass systems of bearing brackets.

Part	Lumped node mass	Ratio between lumped and bearing bracket mass
Upper rotor spider	2000 kg	Approx. ¼
Lower rotor spider	12500 kg	Approx. ½
Turbine cover and bearing bracket	13250 kg	Approx. ¼

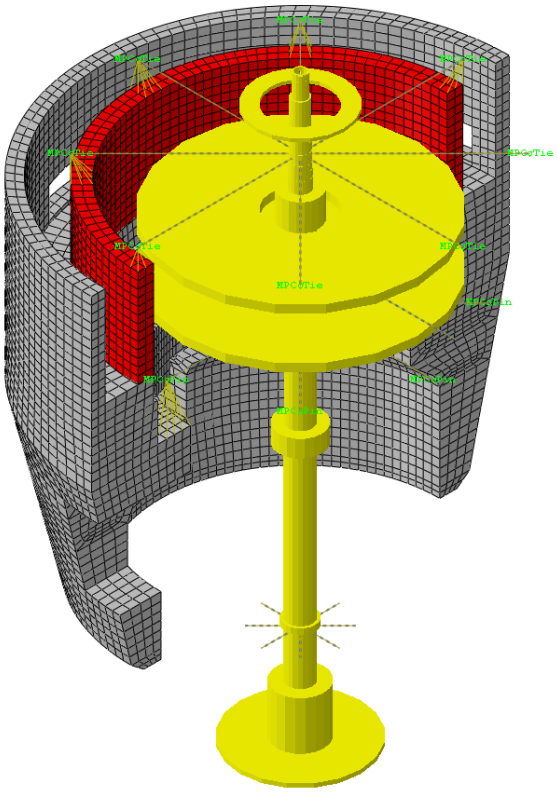

Figure 4—8: Coupled generator and foundation model with elements representing added rotational inertia also shown. Note that the shaft diameter is scaled down and not shown with correct dimensions.

An eccentric mass is connected to the shaft near mid-height of rotor to account for the unbalanced force. This eccentric mass is 48 kg and placed at a distance equal to 4.0 m from the shaft's centre. This result in an eccentric force equal to twice the recommended value given by G6.3 discussed earlier in section 4.1.

4.3.6 Boundary conditions

The FE model of the foundation is constrained to translations in vertical and radial direction in the bottom. At the top and middle part, the foundation is partly constrained since the connecting floor structures do not fully prevent motions of the concrete foundation. Radial springs are defined to simulate this elastic boundary in the FE model. The stiffness of these springs is relatively low in order to allow for displacements of the foundation, with one element introduced at each node in three rows in the circumference at both the top and middle part of the foundation. These springs are assigned with a stiffness of 500 or 1000 N/m in radial direction according to Malm et al. (2013), where the higher stiffness is assigned to the connectors belonging to a middle row and the lower stiffness to the remaining rows. The boundary conditions for the concrete foundation are illustrated in Figure 4—9, and they are identical as for the previous FE analyses performed by Malm et al. (2013). Furthermore, the spring elements representing the turbine bearing bracket's stiffness are placed between the turbine bearing and ground, with the ground point restrained in all directions.

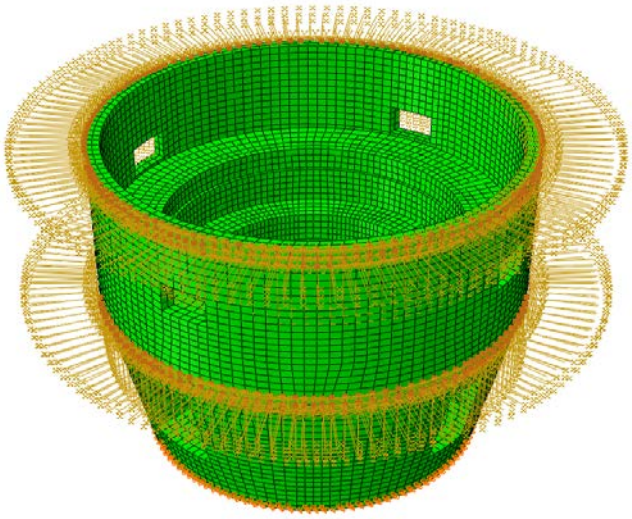

Figure 4—9: Structural boundary conditions.

4.3.7 Load sequence

The foundation and stator parts are initially subjected to gravity load, where the initial static stresses are determined. This static simulation also includes the vertical load from the shaft and rotor acting on the lower rotor spider supports.

The duration of the following dynamic simulation steps are chosen to obtain stabilized numerical results, and also a representative steady state solution. In the numerical analysis it is necessary to avoid initial instability of the shaft at low rotational speeds. Therefore, deformations in the bearings are not allowed during initiation of the shaft rotation in the dynamic analyses. The radial degrees of freedom for the bearings are activated when the shaft reaches a rotational velocity equal to 75 RPM (7.8 rad/s), and the shaft and

its bearings are then allowed to stabilize during a constant rotational velocity. The rotational velocity is then increased to 150 RPM (15.7 rad/s) by an applied torque to the shaft. The tangential magnetic load acting on the stator is applied as a traction force at the inner surface of the stator part when the rotating speed of 150 RPM is reached. The load sequence is compiled in Table 4—10 below.

Table 4—10: Load sequence.

Analysis step	Description
Static analysis	Dead weight, incl. vertical load at the rotor spider supports. Propagated to all the following steps.
Rotation initiation, step time 0.2 s	An increase of the rotational speed to 75 RPM with prescribed zero horizontal movement at bearings.
Shaft stabilizing, step time 0.8 s	A constant rotational speed of 75 RPM with bearings and structure interaction activated.
Rotation increase, step time 5.0 s	An increase of the rotational speed to 150 RPM with bearings and structural interaction activated.
Constant rotation speed of 150 RPM, step time 9.0 s	A constant rotational speed of 150 RPM with bearings and structure interaction activated. Activation of tangential force on stator surface.

4.3.8 Cracked concrete foundation

The earlier study performed by Malm et al. (2013) showed cracking of the concrete foundation caused by temperature effects and drying shrinkage of the concrete during the life span of the hydropower generator. These earlier results are incorporated in the model by introducing cracked concrete elements, i.e. elements with a reduced stiffness. See Figure 4.10. Note that stresses and strain due to thermo-mechanical load and drying shrinkage are not included in the model. Furthermore, the occurrence of a dominating crack close to one of the rotor spider supports is also analysed, with the foundation model shown in Figure 4—1 1. This simulation methodology allows for studies of the influence of a cracked foundation on the induced stresses in the foundation. The parts of the foundation with reduced stiffness may induce increased stress levels in other parts of the structure, and also increased radial movements of the rotating shaft.

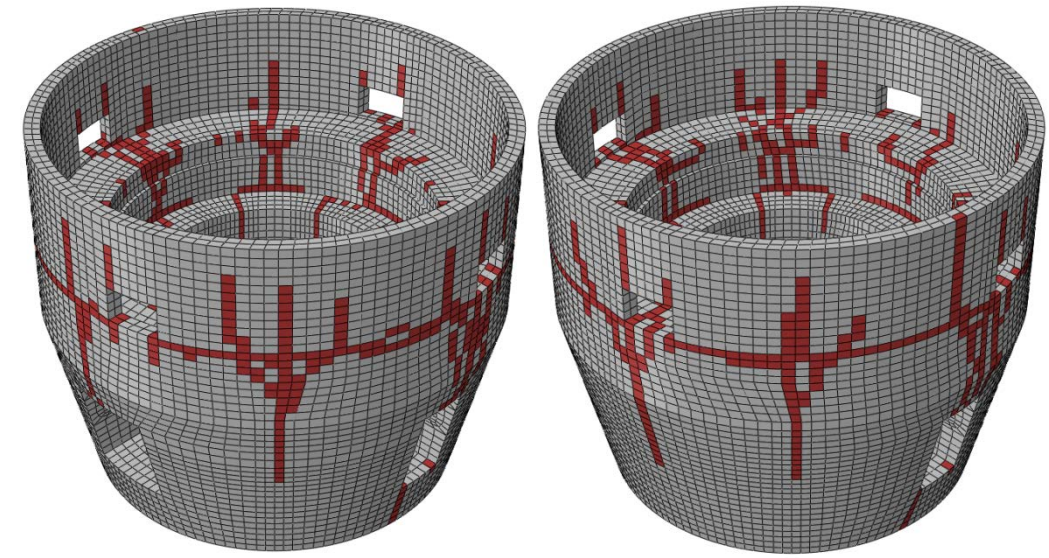

Figure 4—10: Cracked concrete foundation based on Malm et al. (2013), with weaker elements shown in red.

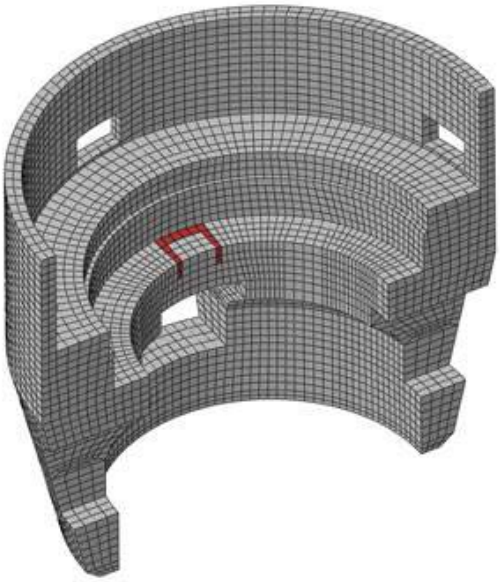

Figure 4—11: Cracked rotor spider support, with weaker elements shown in red.

5 FE analysis results

Eigen frequencies analyses are presented for both the rotating system, i.e. shaft, generator and runner, and the concrete foundation. Furthermore, the results for FE analyses with the rotating generator model coupled to the concrete foundation are presented for both un-cracked and cracked foundations.

5.1 Rotor dynamical FE analysis results

The calculated frequency response for the Abaqus analysis for the first three deformation modes show almost identical results as the frequency analysis for the RAPPID rotor dynamic model, see Table 5—1. The lowest resonance frequencies are approximate 5.3 Hz and 5.5 Hz for the Abaqus and RAPPID analyses, respectively. However, the discrepancies between the models are somewhat greater for the higher frequencies. The frequencies are calculated for a case without rotation for both analyses. Rotation of the shaft will change the natural frequencies for a rotor dynamic analysis due to influence of the gyroscopic moments, see Nässelqvist (2012).

Table 5—1: Eigen frequencies for rotor dynamic model.

Mode number	RAPPID rotor dynamic analysis	Abaqus FE analysis
1	5.48 Hz	5.28 Hz
2	16.37 Hz	15.83 Hz
3	22.62 Hz	22.53 Hz
4	37.07 Hz	32.98 Hz
5	53.18 Hz	48.80 Hz

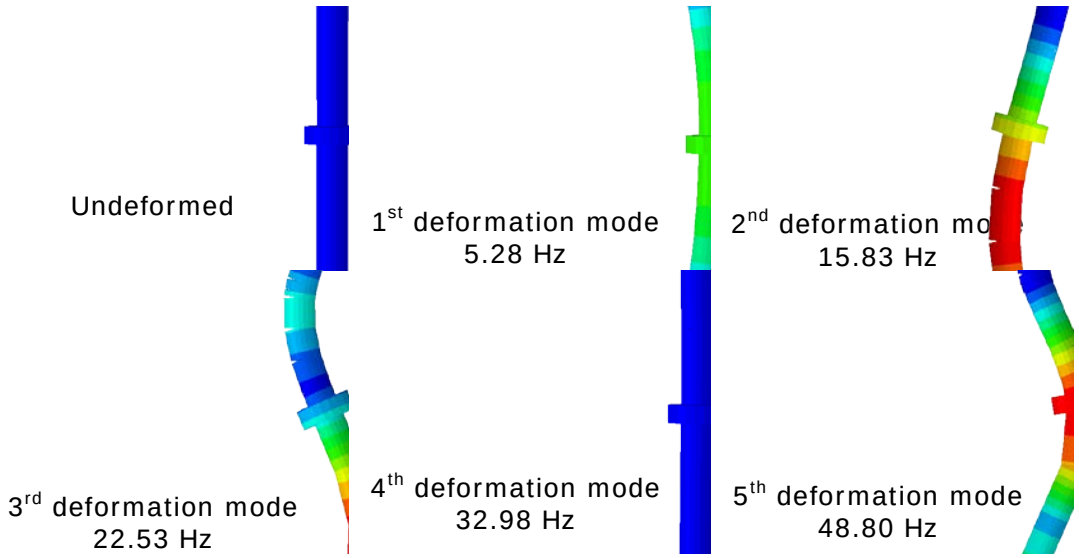

Figure 5—1: Mode shapes for Abaqus rotor dynamic model.

5.2 Coupled structure interaction FE analysis results

The results from the analyses of the coupled generator and foundation model are presented in the following sections, with descriptions of the models given earlier section 4.3. First, results from a frequency analysis of the concrete foundation are presented in section 5.2.1 for comparison with the rotor dynamic analysis presented in section 5.1. The results from the direct time integration analysis of the coupled model are presented in section 5.2.2

5.2.1 Frequency response of structural model

A frequency analysis has been performed on a model which only includes the concrete elements, i.e. an unreinforced foundation. This since connection between the reinforcement elements and the concrete elements caused spurious Eigen frequencies and modes. The first ten Eigen frequencies for the three foundation models are presented in Table 5—1. The mode shapes corresponding to the two lowest Eigen frequencies are shown in Figure 5—1 to Figure 5—3, for the three models.

Comparing the Eigen frequencies of the concrete foundation to those of the rotor model, it can be observed that the lowest frequency of the rotor model is approximately a factor 5 lower than that of the concrete foundation. Furthermore, it can also be observed that the frequency of the operational load is significantly lower than the lowest frequency of the concrete foundation. The operational load has a dominating frequency of 2.5 Hz corresponding to the rotational speed, i.e. approximately a factor 10 lower than the concrete foundation. However, non-circular generator parts, i.e. stator and rotor, and the runner are likely to induce higher frequencies to the system. Typically, the dominating frequencies induced by these phenomena are two and five to six times higher than the dominating frequency for the operational load of 2.5 Hz given above, respectively.

Table 5—1: First ten Eigen frequencies of the concrete foundation model.

Mode number	Un-cracked	Cracked	Cracked 2
1	30.47 Hz	25.56 Hz	30.47 Hz
2	31.09 Hz	27.11 Hz	31.02 Hz
3	37.04 Hz	27.59 Hz	36.78 Hz
4	38.38 Hz	27.77 Hz	38.18 Hz
5	44.47 Hz	29.52 Hz	44.45 Hz
6	44.52 Hz	30.01 Hz	44.51 Hz
7	47.98 Hz	33.35 Hz	47.97 Hz
8	48.91 Hz	34.50 Hz	48.91 Hz
9	49.39 Hz	42.43 Hz	49.38 Hz
10	59.59 Hz	43.30 Hz	59.58 Hz

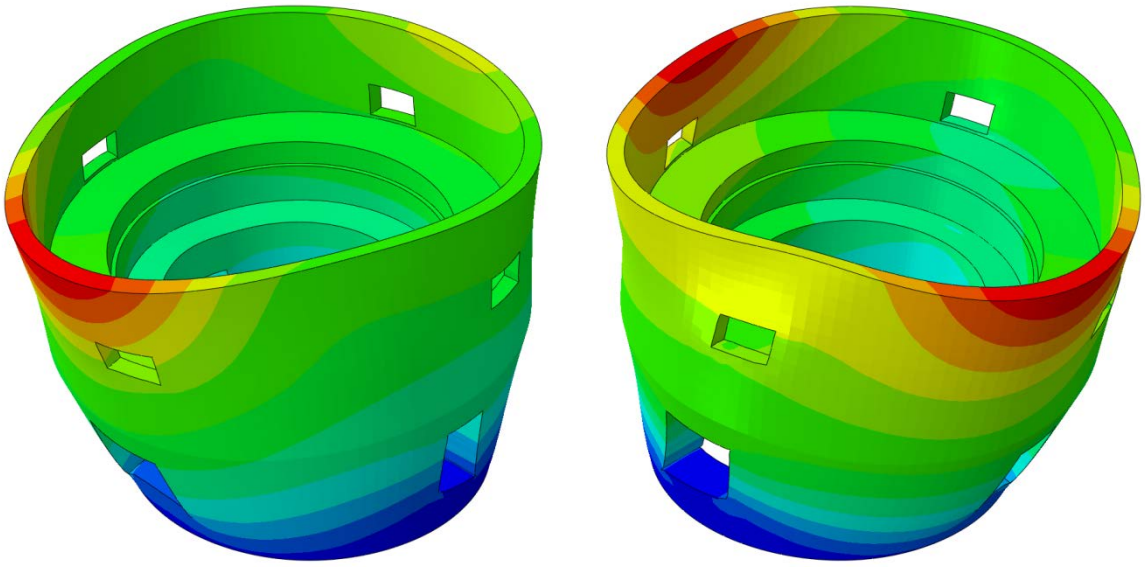

a) 1st mode, 30.47 Hz b) 2nd mode, 31.09 Hz

Figure 5—1: Mode shapes of the un-cracked model.

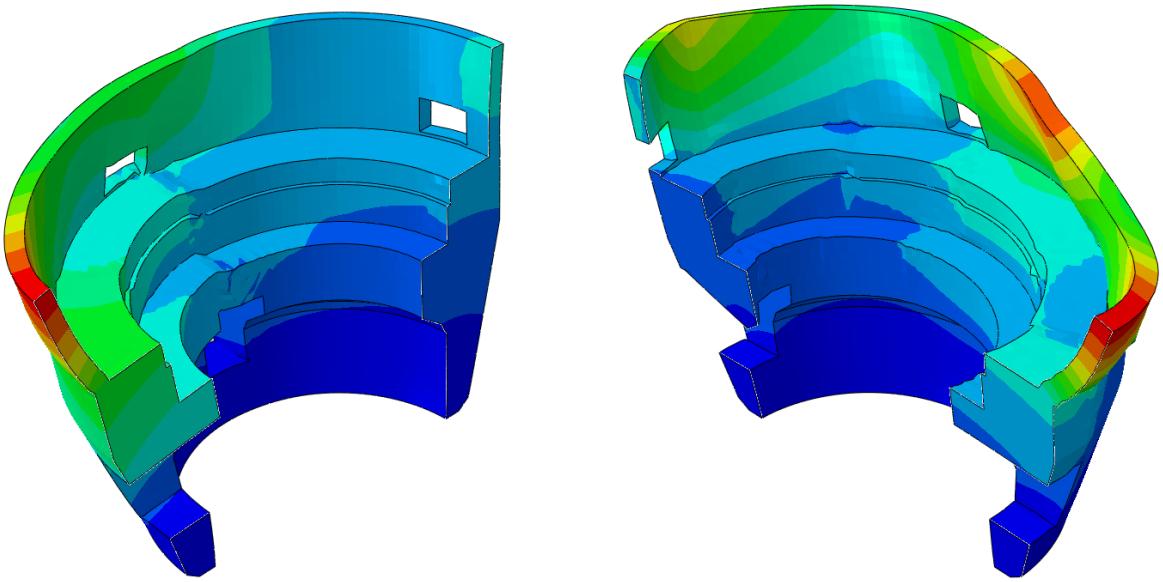

a) 1st mode, 25.56 Hz

b) 2nd mode, 27.11 Hz

Figure 5—2: Mode shapes of the cracked model. Model with distributed cracks according to Figure 4—10.

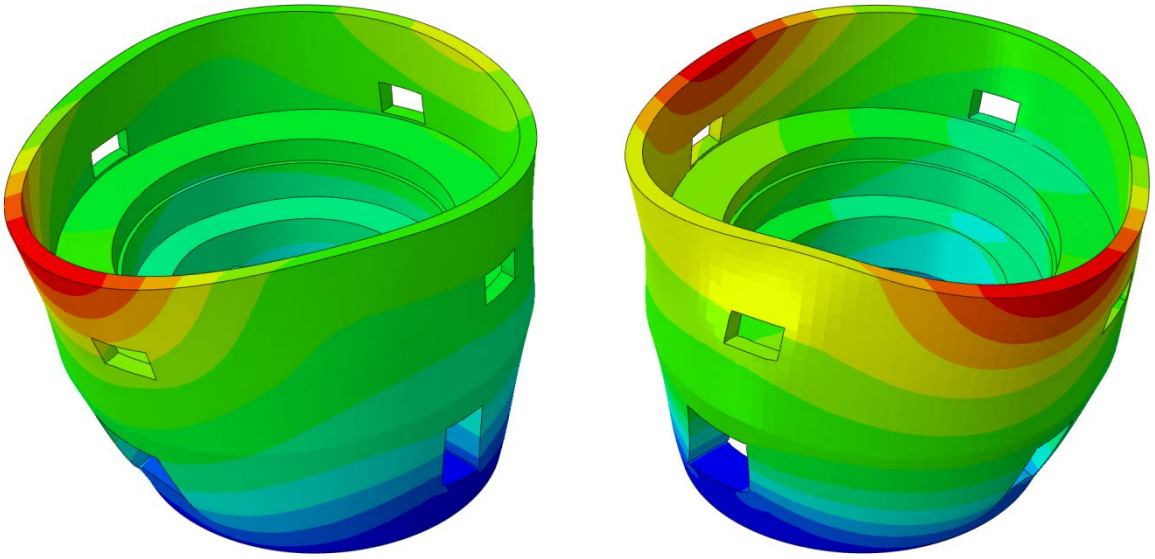

a) 1st mode, 30.47 Hz

b) 2nd mode, 31.02 Hz

Figure 5—3: Mode shapes of the cracked model. Model with a single crack according to Figure 4—11.

5.2.2 Direct time integration results

Results from the direct time integration analyses are presented below for the three models described in section 4.3.

Bearing and bearing bracket forces

A time history of the forces in the three guide bearings is shown in Figure 5—4. The forces from the three different models are quite similar and the un-cracked model and the model with a single crack (cracked 2) are almost identical when constant rotational speed of 150 RPM is reached after approximate 7 s. The model with distributed cracks shows a disturbance in the load in all bearings during the first seconds after constant rotational speed of 150 RPM is reached, this disturbance is, however, cancelled out as the loads are stabilized at a slightly lower level than the other two models.

The radial guide bearing force and its angle in the global system for the upper bearing is shown in Figure 5—5, for the portion of the time history when constant rotational speed of 150 RPM is reached; from 7 to 16 s. It can be observed that the differences between the three models are small and that only the model with distributed cracking shows some scattering in the load level. The disturbance in this model observed in Figure 5—4 is also shown in Figure 5—5, where the load curve deviates from the otherwise circular pattern. This circular pattern differ from measured bearing forces, see Figure 2—4, due to the simplified bearing properties.

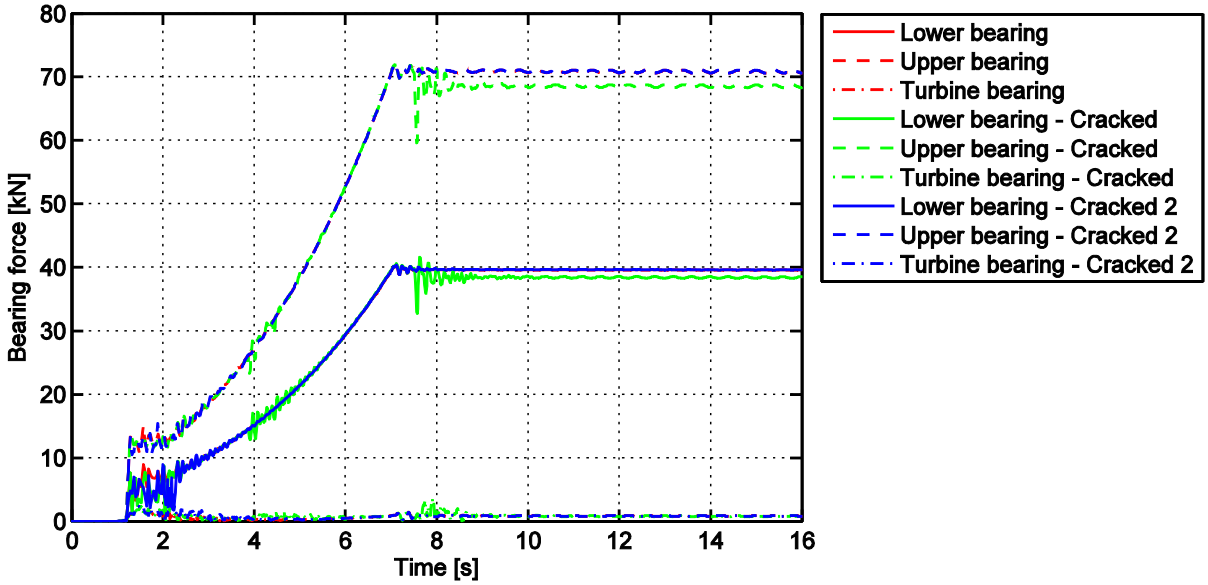

Figure 5—4: Guide bearing loads, with the torque on the stator applied after 7 s in the diagram.

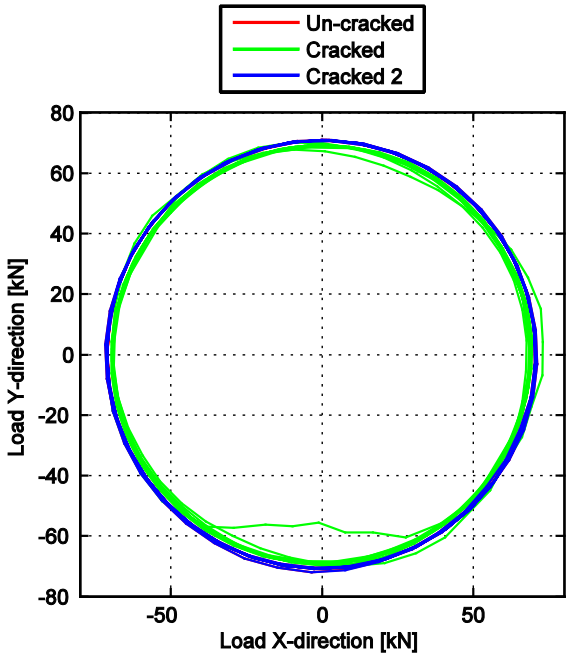

Figure 5—5: Radial load in the upper guide bearing.

The guide bearing forces are in the FE model transferred to the concrete foundation through the upper and lower rotor bearing brackets, that each consists of 8 beams in the numerical model. To study how the change in guide bearing forces translates to the change in load on the foundation, the force in two of the beams in the lower bearing bracket is shown in Figure 5—6 for all three models. The two beams are located in the positive global z-direction (bracket no. 3) and the negative global z-direction (bracket no. 7). It should also be noted that bracket no. 3 is attached to the support which is surrounded by a crack in the cracked 2 model. All three models show similar load levels throughout the entire analysis. To further study the small differences that are present in load levels, the last second of the analysis is presented in Figure 5—7 for the same brackets as in Figure 5—6. In this figure it can be seen that loads follow the operation frequency of the rotor and the periodic return of the load is not influenced by the cracks introduced in the foundation. The amplitude is, however, slightly altered by the introduction of cracks, especially for the foundation with distributed cracks.

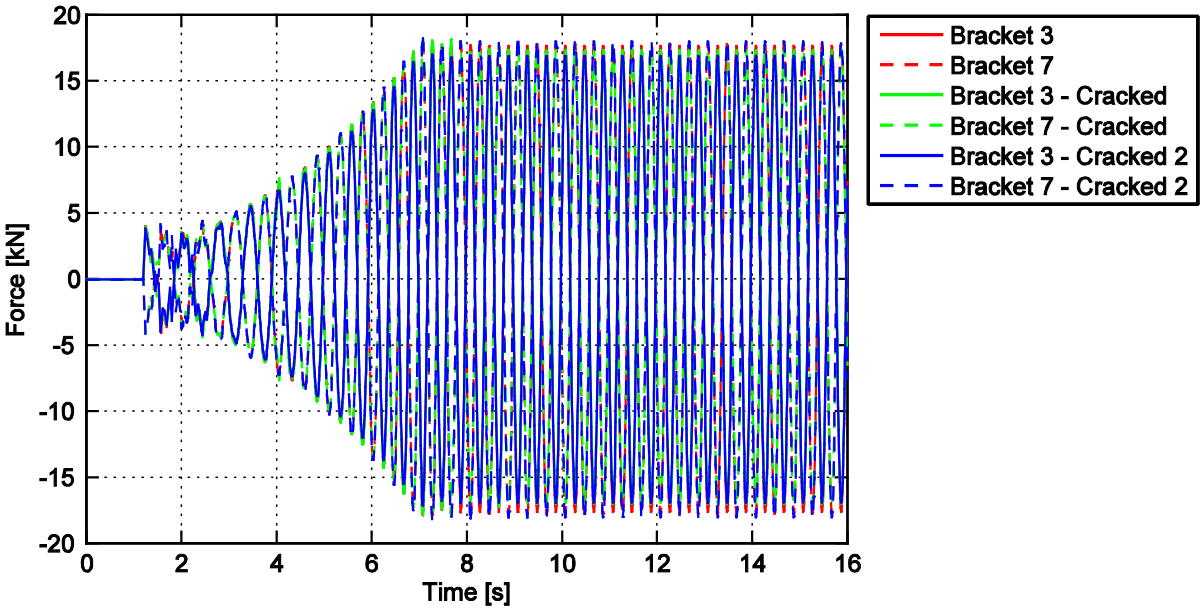

Figure 5—6: Time history of forces in two opposite supports of the lower bearing brackets. The torque on the stator is applied after 7 s in the diagram.

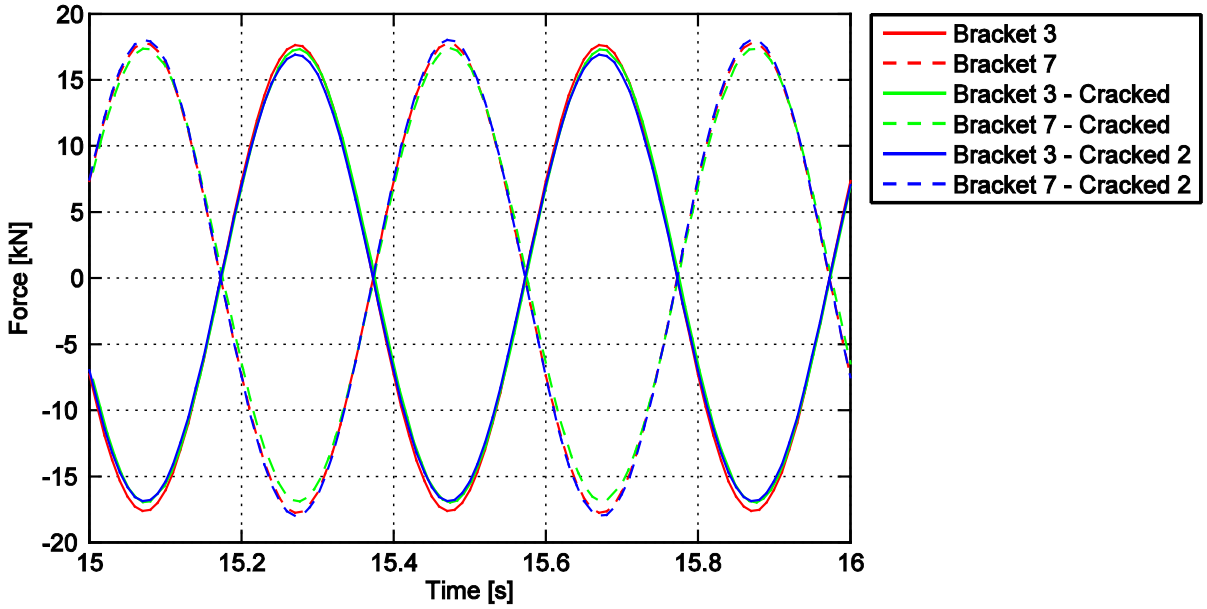

Figure 5—7: Time history of forces in two opposite supports of the lower bearing brackets, zoomed in at the last second of the steady state.

To summarise the forces in the two bearing brackets connected to the analysed part of the concrete structure, the maximum and minimum force in each bracket is presented in Table 5—2 and Table 5—3 for the upper and the lower bearing bracket, respectively. It should be noted that bracket 1 coincides with the global x-axis, see for example Figure 4—3, and for each increase in number the bracket is rotated 45° clockwise.

Table 5—2: Forces in the upper rotor bearing bracket, [kN].

Bracket no.	Un-cracked		Cracked		Cracked 2	
	Max	Min	Max	Min	Max	Min
1	10.05	-9.88	11.35	-9.55	10.07	-9.89
2	9.80	-10.29	9.78	-10.42	9.80	-10.32
3	9.91	-9.82	9.54	-10.75	9.94	-9.85
4	10.28	-10.07	11.65	-10.05	10.30	-10.08
5	9.88	-10.06	11.23	-9.91	9.88	-10.07
6	10.22	-9.86	9.91	-10.28	10.23	-9.88
7	9.99	-9.88	9.80	-10.25	9.99	-9.89
8	10.07	-10.22	10.07	-11.29	10.09	-10.24
Max Range	20.35		21.70		20.38	

Table 5—3: Forces in the lower rotor bearing bracket, [kN]. The red cell indicates the support with the crack in the last model.

Bracket no.	Un-cracked		Cracked		Cracked 2	
	Max	Min	Max	Min	Max	Min
1	17.75	-17.91	17.58	-19.25	17.77	-17.91
2	17.63	-17.92	17.43	-19.07	17.74	-18.08
3	17.78	-17.88	18.16	-17.80	17.04	-17.12
4	17.78	-17.98	18.31	-17.93	17.91	-18.10
5	17.91	-17.75	17.48	-18.64	17.91	-17.77
6	17.76	-18.04	16.94	-19.22	17.91	-18.18
7	18.02	-17.91	18.19	-17.73	18.28	-18.16
8	18.22	-17.62	18.79	-18.07	18.37	-17.74
Max Range	35.93		36.86		36.43	

Concrete stresses

To study the impact from the rotor dynamic load on the concrete foundation the distribution of the maximum principal stress is shown in Figure 5—8 to Figure 5—10 for the three FE models. From the un-cracked foundation model in Figure 5—8 it is observed that the difference between the stress state of the foundation after gravity loading, Figure 5—8a), and at steady-state condition of the rotor, Figure 5—8b), is very small. This stress increase at the stator support can probably be contributed to the torsional moment applied to the stator, which is created when the generator is magnetised. The same tendency can also be observed for the model with distributed cracks, Figure 5—9, but with at a higher stress level and further increased stresses due to the rotor dynamic loads. Again, this is most prominent at the stator supports due to torsional moment. The model with a single crack around one of the supports at the lower bearing, Figure 5—10, show an almost identical stress distribution as the un-cracked model, apart from the area around the cracked support. But no significant increase in stress is found around this support or the adjacent support due to the rotor dynamic load. Furthermore, the maximum tensile stress increases from approximate 1.0 MPa, for the un-cracked model, to approximate 1.9 MPa for the cracked models. The reason for this is the unloading of the cracked elements, and subsequent increased loading of the intact part of the foundation. However, the calculated magnitudes for these tensile stresses are still below the strength of the concrete.

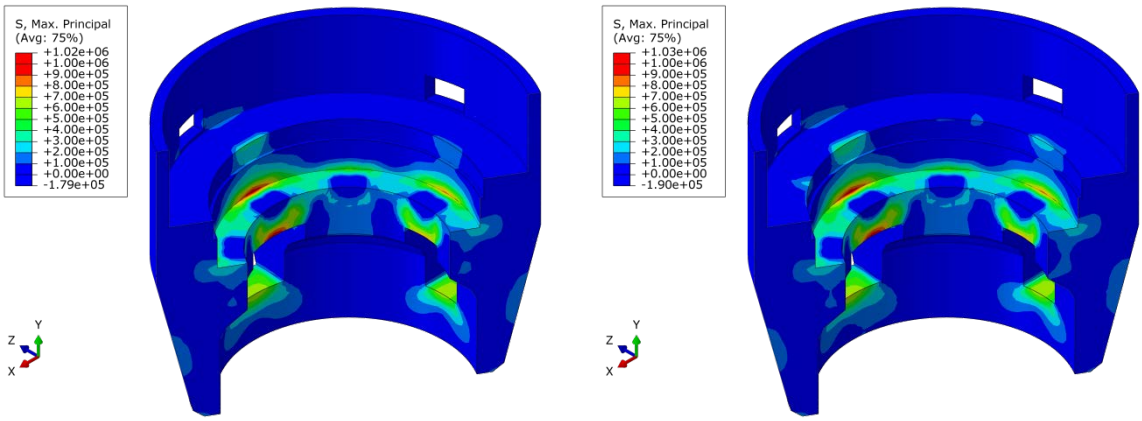

a) Gravity loading b) Steady state

Figure 5—8: Contour of the maximum principal stress [Pa] for the un-cracked model.

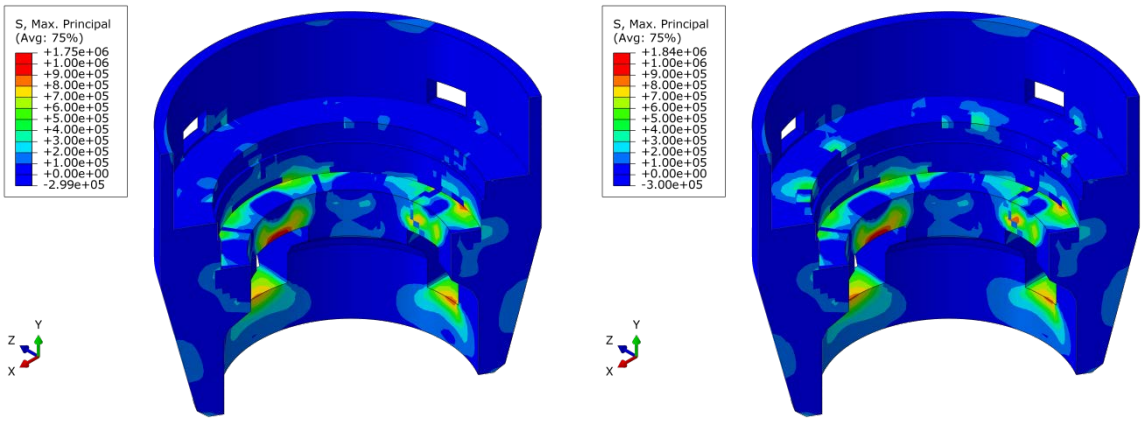

a) Gravity loading b) Steady state

Figure 5—9: Contour of the maximum principal stress [Pa] for the model with distributed cracks according to Figure 4—10.

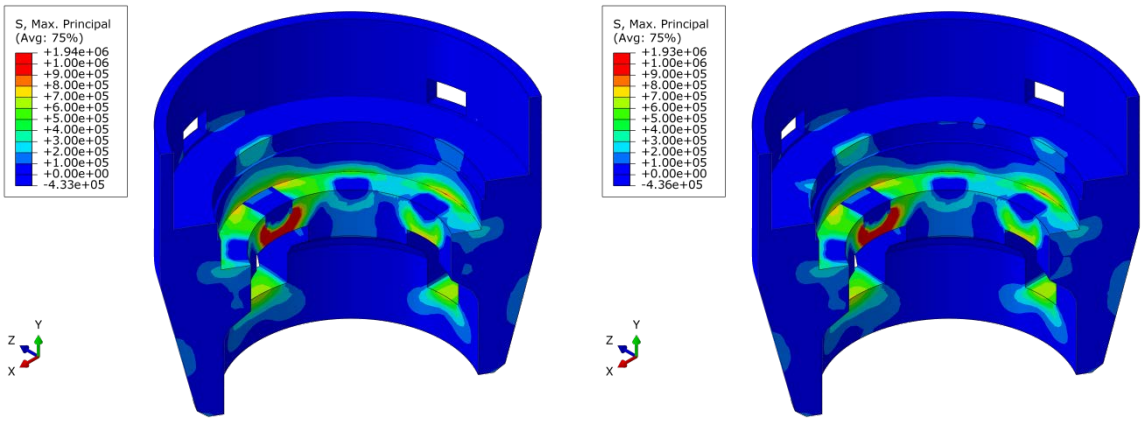

a) Gravity loading b) Steady state

Figure 5—10: Contour of the maximum principal stress [Pa] for the model with a single crack according to Figure 4—11.

In Figure 5—11 to Figure 5—14 the time history of the maximum principal stress is shown for elements that show high stress in the concrete surrounding three different supports of the lower bearing bracket. The element is chosen as the element that exhibits the highest stress at its integration point and can thus differ between the different models. As the stress is calculated and plotted at the integration point of the element it should be noticed that the surface stresses can be somewhat higher than the stresses shown in the time histories

Figure 5—11 shows the stress in an element near the support for bracket no. 3 of the lower bearing bracket, this is the support that is cracked in the cracked 2 model. In Figure 5—11a) the total value of the stress is shown, where the model with the single crack shows the highest stress. But it can also be observed that most of the stress magnitude is due to the static loads. What should also be noted is that in the un-cracked and distributed crack models, the area with the highest stress is located at the back of the support close to the corner, whereas for the single crack model this area is unloaded by the crack and the stress concentration is located further within the volume of the concrete. Looking at the variation in stress due to the rotor dynamic load, Figure 5—11b), it can be observed that the un-cracked model and the model with distributed cracks show significantly increased stress variations compared to the model with a single crack. Especially the model with distributed cracks shows a large increase when the torque is applied. This is probably due to loads being redistributed to other brackets and also transferred across the crack through the reinforcement. It should be noted the stresses are not extracted from one of the cracked concrete elements, which are likely to show lower stresses due to their reduced stiffness. The introduction of cracks in the concrete foundation not only reduces the stiffness of the supports for the generator, but also locally changes the stresses within the foundation, and for the cracked 2 model relocates the stress concentration further away from the support. Furthermore, the concrete stresses near the cracked support in the model cracked 2 is reduced due to the decreased

stiffness of this support, and the dynamic load is therefore transferred to the other stiffer supports, see Table 5—3.

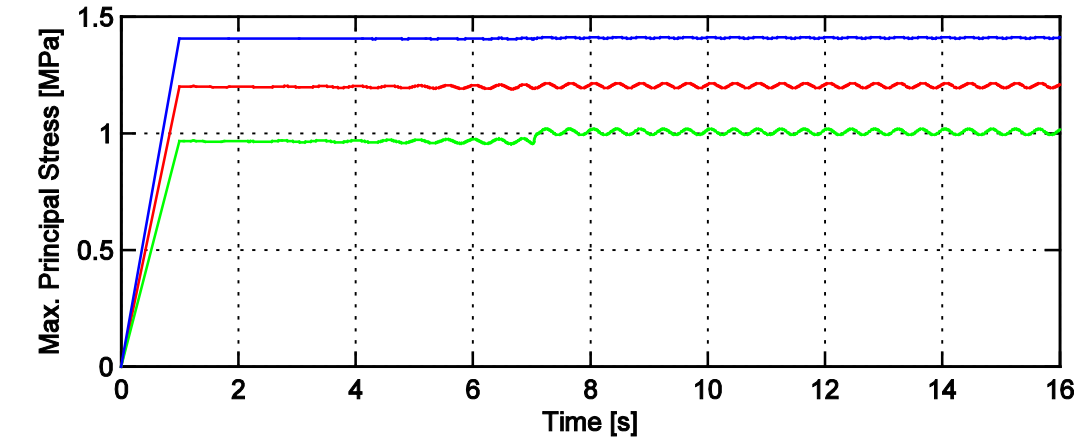

a) Maximum principal stress

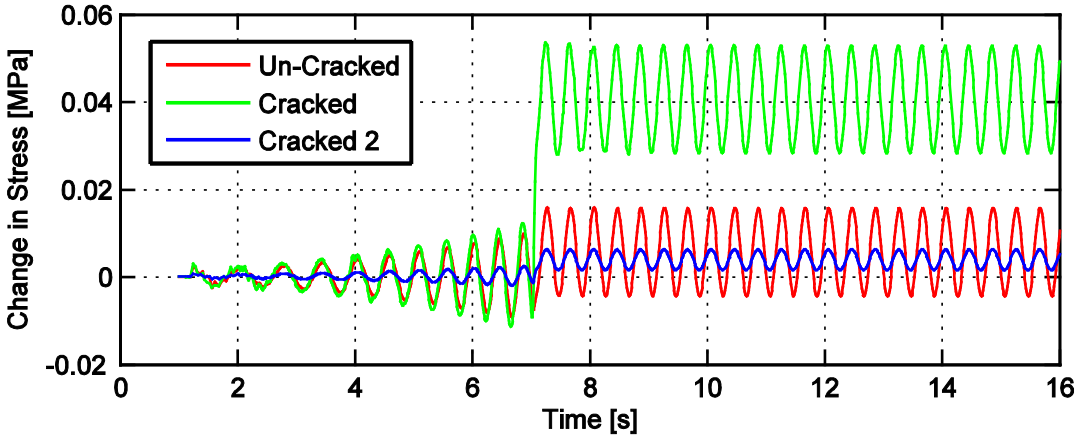

b) Change in maximum principal stress

Figure 5—11: Time history of maximum principal stress in the elements around the support for bracket no. 3 in the lower bearing bracket. The torque on the stator is applied after 7 s in the diagram.

As could be observed in the contour plots of the stress state in Figure 5—8 to Figure 5—10, the area with the highest stress is located above the large penetration through the foundation. This penetration is located below bracket no. 3 and to further examine this area the time history of the stress is shown in Figure 5—12. As can be observed in the figures, a large portion of the stress is due to the static load, where the stresses due to the dynamic load are only about 0.5 % of the static loads. It can also be observed that the torque applied when the generator is magnetised unloads this area whereas it increases the load in the area closer to the support. However, the cracked 2 model shows almost the same dynamic behaviour at both locations.

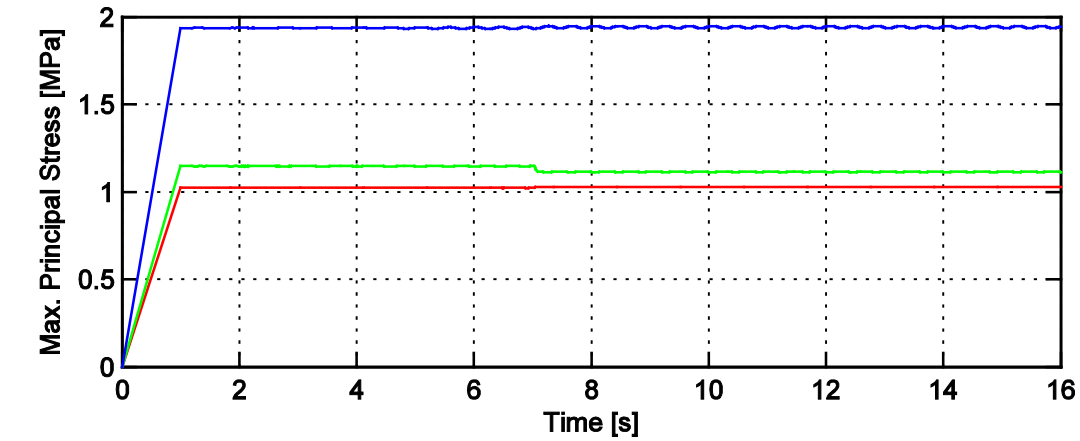

a) Maximum principal stress

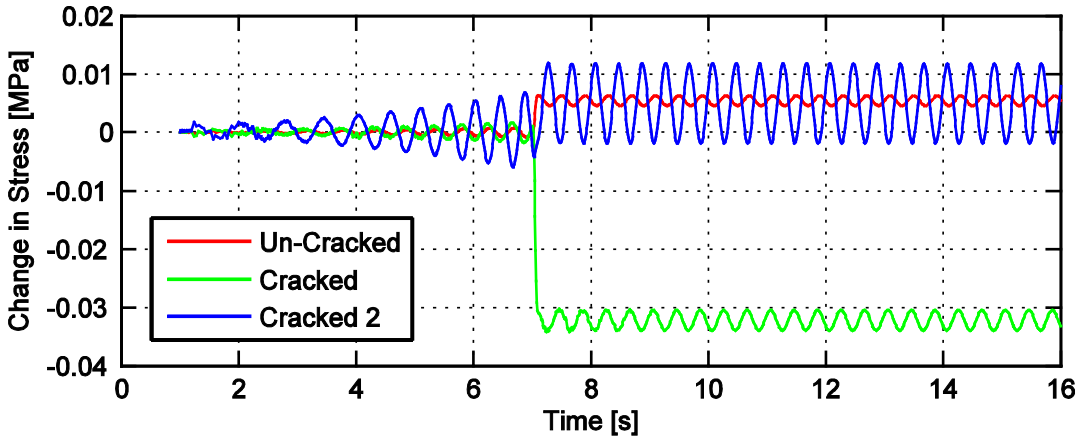

b) Change in maximum principal stress

Figure 5—12: Time history of maximum principal stress in the elements above the penetration at support for bracket no. 3. The torque on the stator is applied after 7 s in the diagram.

To compare the stresses in bracket no.3 with a similar support that is also situated above a penetration, although a smaller one, the time history of the stresses at bracket no. 5 is shown in Figure 5—13. As for bracket no.3 most of the stress magnitude is due to static loads and the stress variation due the rotor dynamic loads are similar, except for the large increase due to the torque applied to the stator for the distributed crack model. A large radial crack is located close to this support and it is going through the whole cross-section of the foundation which might explain the large increase due to the torque. In fact, the element with the highest stress is located adjacent to this crack. For the two other models the highest stress is obtained behind the support at the corner, as for bracket no. 3.

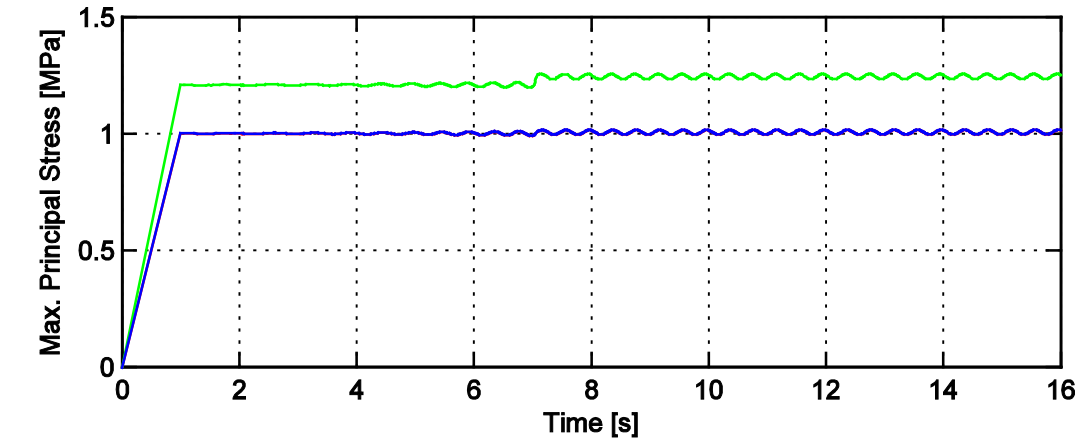

a) Maximum principal stress

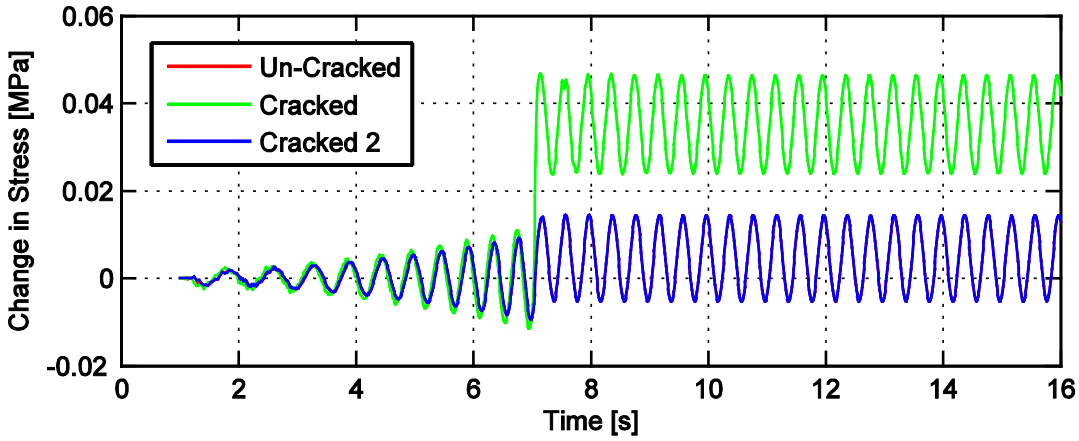

b) Change in maximum principal stress

Figure 5—13: Time history of maximum principal stress in the elements around the support for bracket no. 5 in the lower bearing bracket. The torque on the stator is applied after 7 s in the diagram.

Figure 5—14 shows the stress in an element around the support for bracket no. 7 of the lower bearing bracket, opposite bracket no. 3. No penetration is located below this support. At this support the highest stress is exhibited in the un-cracked and the cracked 2 model with a single concrete crack. These two models show similar stress states at this support, which can be expected since the cracked 2 model is basically identical to the un-cracked model, except for the introduced single crack around the support for bracket no. 3. The model with distributed cracks exhibits lower stress compared to the other two models near this support and at the same element as the two other models shows the highest stress the stress is only a tenth in this model. This is due to the redistribution of stresses where the highest stress in this model occurs adjacent to one of these cracks. Looking at the variations in stress due to the rotor dynamic load, Figure 5—14b), the distributed crack model shows a little higher variation of the stresses than the other two models for this support. This could also be explained by the cracks located close to the support in this model, and that the stiffness of the concrete foundation locally is reduced for this model at this support location.

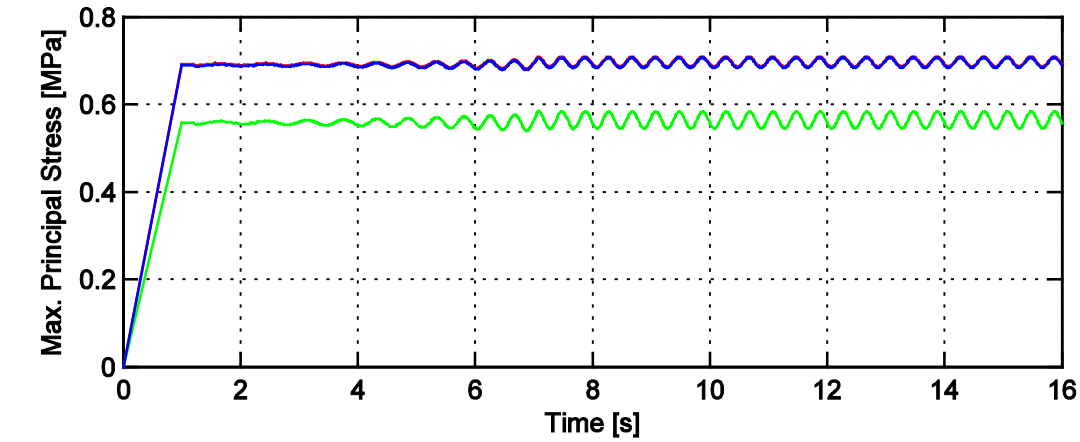

a) Maximum principal stress

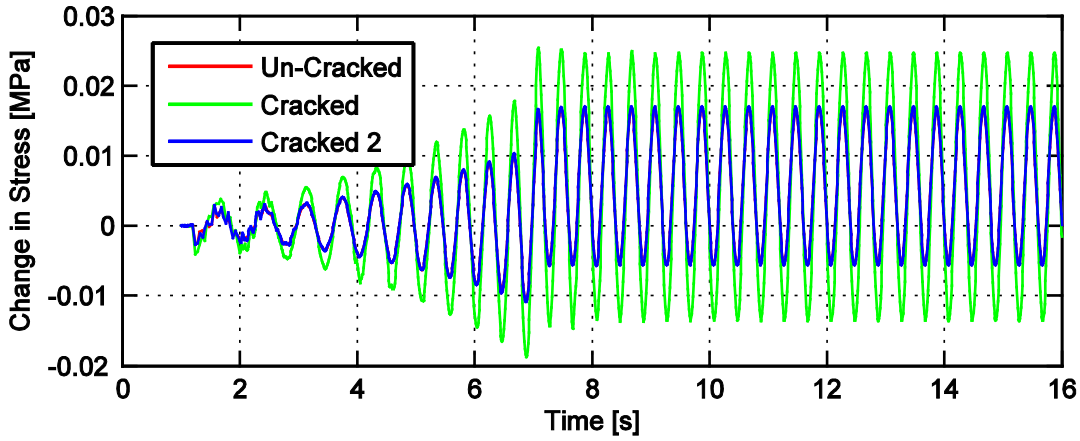

b) Change in maximum principal stress

Figure 5—14: Time history of maximum principal stress in the elements around the support for bracket no. 7 in the lower bearing bracket. The torque on the stator is applied after 7 s in the diagram.

An example of a time history of the maximum principal stress in the concrete around two of the stator support is shown in Figure 5—15, where a) show bracket no. 3 and b) bracket no. 5. Both the un-cracked model and the cracked 2 model shows similar results for both supports, but it can clearly be seen that the different sizes of penetrations below the supports has an influence on the static stress state. The influence of the torque applied when the machine is magnetised is, however, of similar magnitude at both supports for these two models. The distributed crack model show somewhat different results, firstly, as was also observed at the lower bearing bracket, the stress state is much more influenced by the applied torque due to the presence of radial cracks around the supports. It can also be observed since the difference between the static stress state is smaller between the supports, probably also due to radial cracks going through the penetrations and thereby altering the static behaviour of the structure.

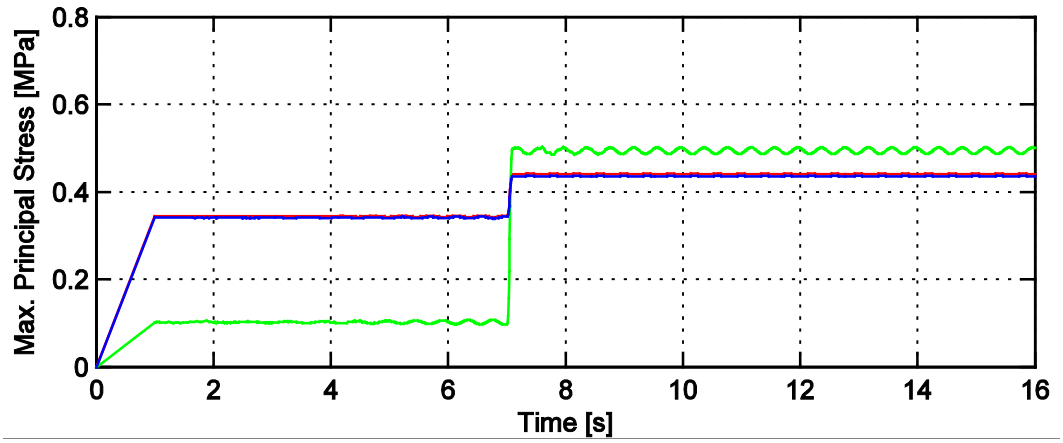

a) Maximum principal stress

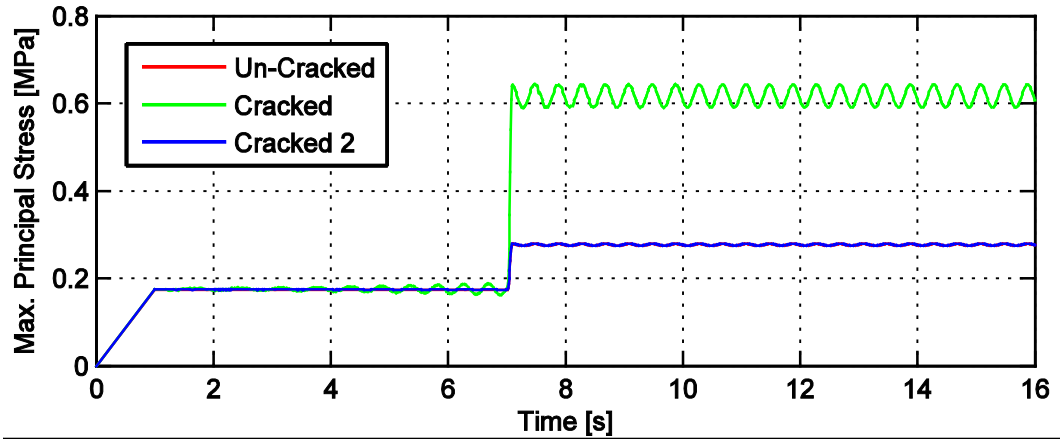

b) Maximum principal stress

Figure 5—15: Time history of maximum principal stress in the elements around the stator support for a) bracket no. 3 and b) bracket no. 5 of the upper bearing bracket. The torque on the stator is applied after 7 s in the diagram.

Through all investigated locations the variation in the tensile concrete stresses are small, typically below 0.1 MPa, but for some locations the absolute value of tensile stress is close to the tensile strength of the concrete given by Larsson (2010); 2.2 MPa. At such static stress levels even a small increase as 0.1 MPa could lead to earlier and further crack propagation, especially if a crack is already initiated in that area. Considering this, it will be important to also include other loads that can increase the stress level, such as temperature variation and other environmental load, in the same model as the rotor dynamic loads.

Reinforcement stresses

It is also important to evaluate the stress in the reinforcement for the models with cracks. The effective stress in the reinforcement is shown in Figure 5—16 and Figure 5—17, for the model with distributed cracks and a single crack respectively. Both figures show the stress state after static loading and when the rotor dynamic loads have reached steady state condition. For the

distributed crack model in Figure 5—16 the same tendencies as for the concrete is found; i.e. the largest increase in stress is observed at the stator support, typically where a crack is located adjacent to a support. It can also be observed that the highest reinforcement stresses in the lower bearing bracket is obtained at bracket no. 5, for the part of the foundation shown in the figure. The highest reinforcement stresses, 38 MPa, is located in the roof of the penetration below bracket no. 5 and can be explained by the radial crack that is located in this area of the foundation. For the model with a single crack, Figure 5—17, the highest reinforcement stresses are located in the cracked elements around bracket no. 3 in the lower bearing bracket; as could be expected. Small differences can be observed between the two shown stress states and only a small increase in the reinforcement stress due to the dynamic load can be observed where no new areas of stress concentration appear.

For both models the dynamic stresses in the reinforcement are very small and the highest observed absolute stress is 38 MPa. This is an indication that the rotor dynamic load during normal operation alone does not give any significant contribution to the fatigue of the reinforcement, even where the concrete is cracked. However, thermal induced stress is not considered for these models, and this is likely to change the calculated stress magnitude.

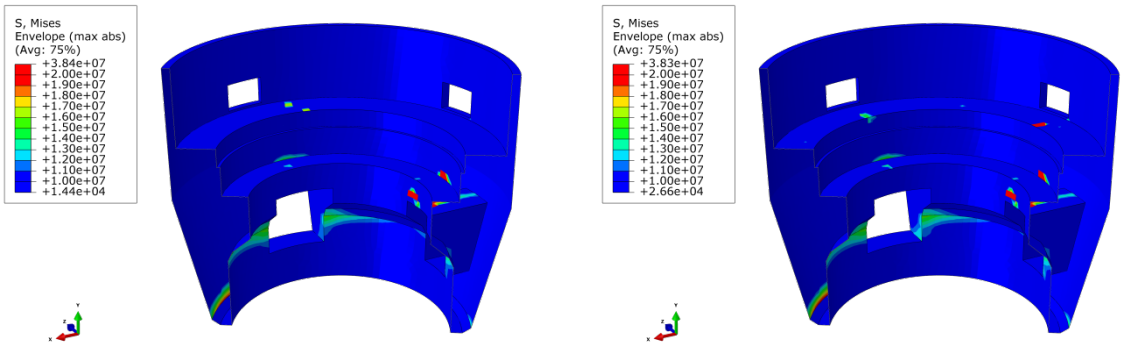

a) Gravity loading

b) Steady state

Figure 5—16: Contour of the effective stress [Pa] in the reinforcement for the model with distributed cracks according to Figure 4—10.

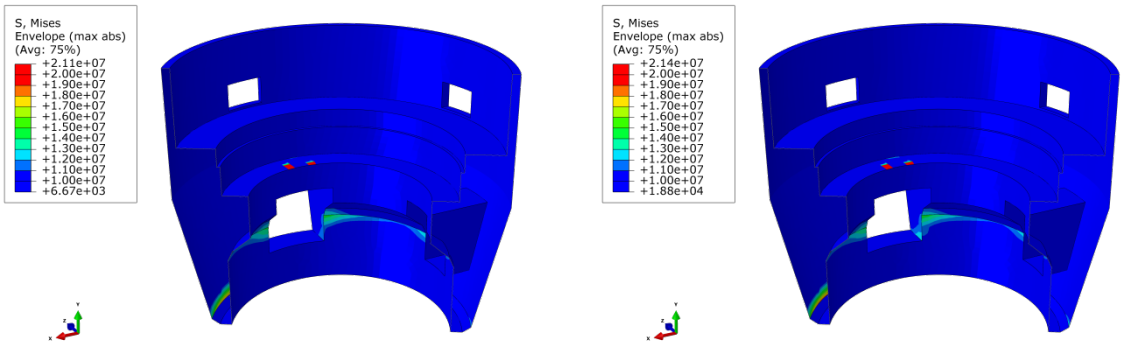

a) Gravity loading b) Steady state

Figure 5—17: Contour of the effective stress [Pa] in the reinforcement for the model with a single crack according to Figure 4—11.

To study the dynamic response in the reinforcement in more detail, time histories of the maximum tensile axial stress found in the reinforcement around two supports are shown in Figure 5—18 and Figure 5—19.

Figure 5—18 shows the tensile reinforcement stress around bracket no. 3 of the lower bearing bracket for the two cracked models. For the absolute values shown in Figure 5—18a) it can be observed that the highest tensile stresses are obtained in the distributed crack model, located in the wall behind the support, where a crack is located. For the single crack model the highest tensile stresses occurs in one of the cracked concrete elements behind the support. Looking at the variation of the stress, Figure 5—18b), it can clearly be observed that the dynamic response in the single cracked model is much higher than the distributed cracked model, almost an increase of 30. This even though the reinforcement stresses are extracted from a cracked concrete element in both models, but since entire support is surrounded by a crack in the single crack model its stiffness reduction is much higher. Also, as was shown for the concrete stresses, the torque gives a significant stress increase for the distributed crack model, due to the radial cracks.

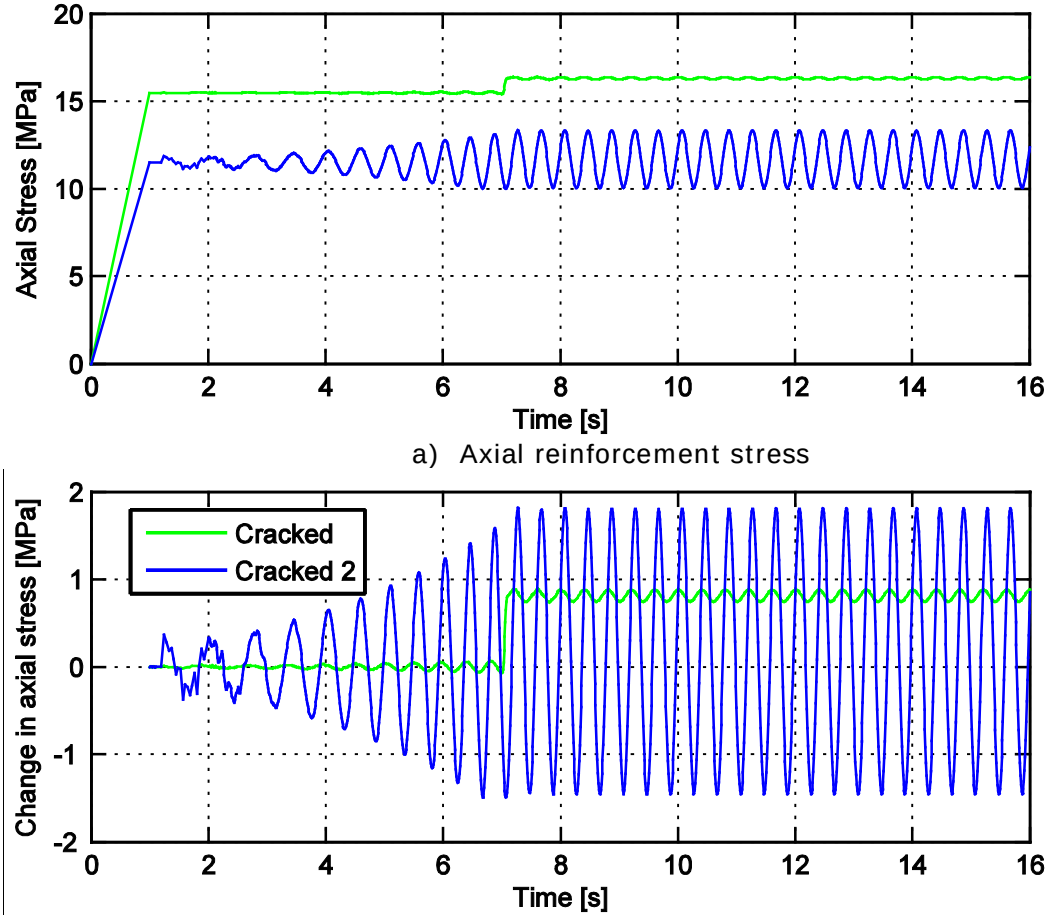

a) Axial reinforcement stress

b) Change in axial reinforcement stress

Figure 5—18: Time history axial stress in the reinforcement around the support for bracket no. 3 in the lower bearing bracket. The torque on the stator is applied after 7 s in the diagram.

In Figure 5—19 the reinforcement stresses near bracket no. 3 in the upper bearing bracket is shown. Here the single crack model is basically un-cracked which is also indicated by the low reinforcement stresses, both regarding the absolute value but especially in the variation in stress. The stress in the reinforcement for the distributed crack model shows similar behaviour as for the lower bearing bracket, Figure 5—18, although the stress magnitude is lower. The variation of the stress is, however, larger and especially the torque gives an increase in tensile reinforcement stress.

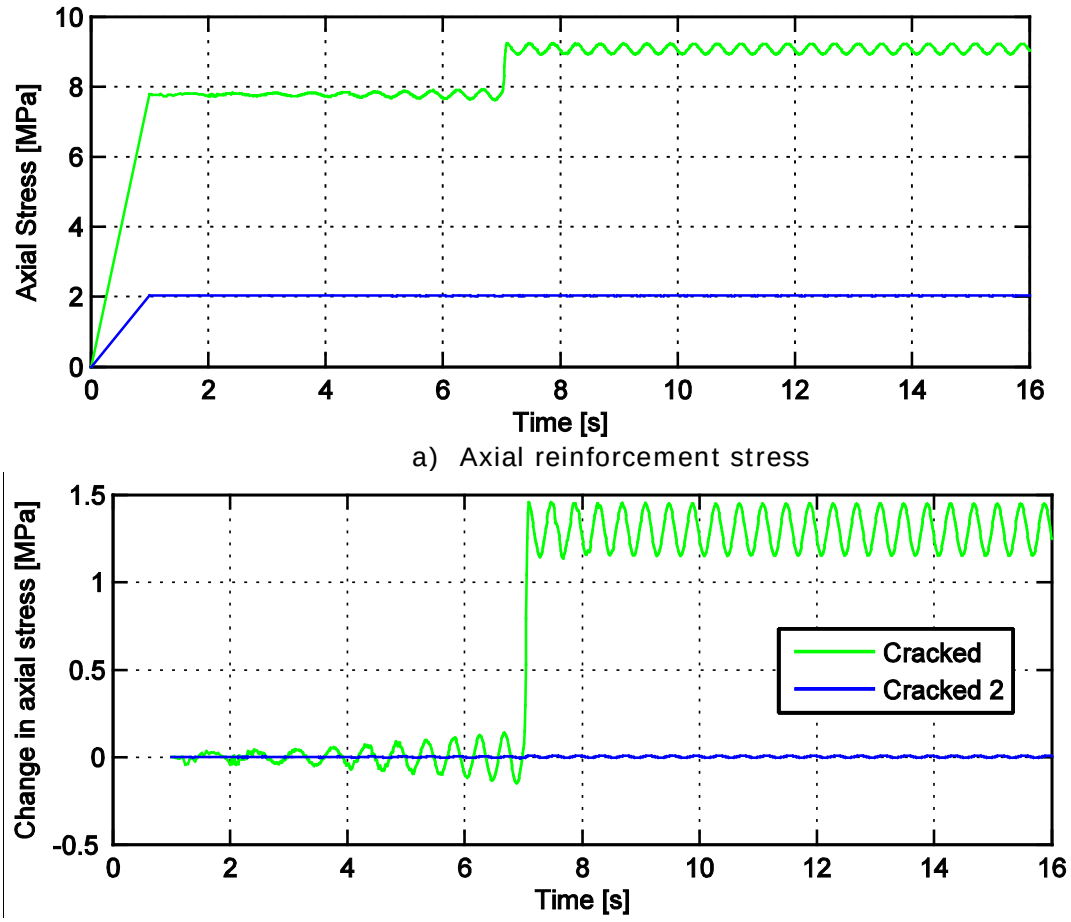

a) Axial reinforcement stress

b) Change in axial reinforcement stress

Figure 5—19: Time history axial stress in the reinforcement around the support for bracket no. 3 in the upper bearing bracket. The torque on the stator is applied after 7 s in the diagram.

6 Discussion

The analyses of the interaction of a hydro power unit with its cracked concrete foundation have raised a number of issues regarding suitable modelling techniques. These are discussed in within the following sections. Furthermore, a PhD project within this research area has recently been initiated at KTH, and several of the identified issues in this report are likely to be addressed within this PhD project in the future. The modelling experience obtained within this project will be valuable for future dynamic analyses of cracked concrete structures. This new PhD project is financially supported by SVC, the Swedish Hydropower Centre.

6.1 Design aspects and fault cases

The design characteristic of a hydro power generator, its supporting structure and its concrete foundation determines the structural interaction between the generator and its foundation. This gives the load characteristic for the concrete foundation. Therefore, it is difficult to make general assumptions regarding the structural interaction of hydro power generators based on the result obtained for one generator, since the units should be more or less considered as individuals. Furthermore, it is necessary to also consider the operating history, operating mode and the condition of the hydro power unit to obtain reliable analysis results.

Some units have design solutions in which the radial forces, from the rotating system, at the upper generator guide bearing are transferred down into the stator frame. For small and medium-sized units, it may be possible to design the unit so that the upper and lower support structure is connected to the stator, which means that only the stator's thermal expansion and dynamic loads from the rotating structure are to be absorbed by the concrete structure (apart from the loads down at the turbine and the turbine guide bearing). The forces from magnetic pull between the rotor and the stator in this case would be absorbed internally within the generator and its supporting structure.

A short circuit increases the torque induced in the stator considerably according to earlier discussion in section 2.1.4. However, the tangential force acting on the stator supports are not influenced to the same extent, since the inertia of the stator and the deformation of its supporting structure limits the maximum force transferred to the foundation. The stiffness of the supporting structure for the stator, and thereby the resonance frequencies for this structure, have a major influence on the actual forces transferred to the concrete foundation. Furthermore, although a short circuit increases the tangential load on the concrete foundation considerably, it is a seldom occurring fault case. The discussion above regarding the influence of the properties of the supporting structure on the response of the foundation also applies to transient loading due to other fault cases, e.g. water hammer. It is therefore important to accurately describe the physical properties of the supporting structure for a generator to be able to model this type of events accurately.

The occurrence of a runaway may result in considerably increase of rotational speed for the shaft. The analysis of this require a good understanding of the dynamic behaviour of the generator, its supporting structure and the concrete foundation, since the systems resonance frequency need to be accurately determined to obtain a reliable analyses result. Furthermore, mechanical faults during operation may induce high loads on the concrete structure, e.g. due to an increased unbalanced force or changes in stiffness of the supporting structure.

6.2 FE model results

The analysis of the simplified rotor model with Abaqus corresponds to an acceptable degree with the RAPPID rotor dynamic analysis, and the Abaqus analyses are therefore considered to give representative results for the rotor dynamic analysis. This rotor model can therefore be used for the analyses of the structure interaction between generator and concrete foundation. The frequency analysis of the foundation results in decreased resonance frequencies compared to the un-cracked foundation, where the lowest eigenmode is decreased from 30 Hz to 26 Hz. Furthermore, the first deformation modes relates to deformations of the upper part of the foundation. Accordingly, it is likely that the interaction with generator mainly is influenced by local stiffness changes for the foundation close to the support areas.

The dynamic analyses with the interaction between generator and foundation use the same boundary condition as earlier models developed by Malm et al. (2013). The boundary condition at the bottom of the foundation does not allow for vertical or tangential movement of the nodes, with a stiffening of the model as a result. However, it is not likely that this influences the local behaviour at the supports due to dynamic loading from the generator. A more detailed modelling of the boundary conditions for the generator foundation would require that the surrounding structures are incorporated in the dynamic model, or that their stiffness is described more accurately. Furthermore, the horizontal forces from the turbine bearing and its bearing bracket are not transferred to the foundation in the FE analyses. An assumption for the performed structural interaction analysis is that the supporting structure for the stator is much stiffer than the upper rotor bearing bracket and the upper rotor bearing. According to this the radial movement of the rotor shaft at the upper bracket is mainly influenced by the properties of this bearing and bearing bracket. A detailed structural model of the stator and its supporting structure should result in a more nuanced analysis, and a detailed model is also required for the analysis of the response of fault cases e.g. short circuit loads.

The properties of the bearings vary with rotational speed and loading, and also with the direction of the displacement for the shaft. The simplified bearing model used for the FE analyses is considered adequate for this study, with the main characteristics of the bearings considered. However, a more advanced bearing model should be used for future detailed analyses of the interaction between generators and their concrete foundations.

The cracked concrete foundation is subjected to small increases of the dynamic forces acting on the support for the lower rotor bearing bracket, compared to the un-cracked foundation. This also applies to the foundation with only one crack at one of the supports, even though the increase of the support reaction is reduced compared to the foundation with the crack pattern determined by Malm et al. (2013), shown in Figure 4—10. Different pre-existing crack patterns for the concrete foundation are likely to influence the structure's interaction with the generator. The cracks from the earlier analyses performed by Malm et al. (2013) are mainly radial cracks, and this may explain the relative small changes in structural behaviour for the cracked and un-cracked foundations. Furthermore, only the crack pattern was imported to the foundation model, and not the strain and stress from the earlier analyses. However, the use of existing crack patterns determined for a generator foundation may be an alternative modelling technique for the FE analysis. This would enhance the possibility to simulate crack propagation within a concrete foundation, and thereby better estimate the need for future maintenance of the concrete structures.

The simulation sequence for the study is chosen to represent the behaviour of rotor-foundation system during the start and at steady state operation of the generator. The study of transient loadings, e.g. the response due to a short circuit or a water hammer, requires an improved modelling technique. This is since the calculated response due to transient loading is considered more sensitive to the properties of the numerical model and modelling technique, i.e. stiffness for the supporting structures, mass distribution and the internal damping of different parts of the model.

The tensile stress levels in the concrete are increased locally near the stator supports for the cracked foundation during operation, compared to the un-cracked foundation. This is likely a result of the combination of the earlier induced radial cracks and the torque induced in the stator during operation. The tensile concrete stress near these supports is likely to be further increased in the case of a short circuit load for the generator. However, the tensile concrete stress in the foundation due to this event is highly dependent on the stiffness of the stator and its load bearing structure as discussed earlier in section 6.1, and an improved analyse of these stresses require a considerably more detailed analyse of the structure and its interaction with the foundation. Furthermore, the analyses show low stresses in the reinforcement for the analysed cases. A combination of earlier load sequences with induced strain due to drying shrinkage and thermally induced stresses in the foundation needs to be combined with future FE analyses of the stress field during operation of a hydro power generator.

A detailed FE model of mechanical components, such as bearing brackets, rotor, bearings and supporting structure for the stator, should improve the FE analysis of structural interaction. However, the modelling of the interaction between the foundation and generator require that the connections between mechanical components and the concrete foundation are described accurately. Furthermore, the properties for these connections may change from their initial, or intended, behaviour during the life span of a generator. This may change the induced stress in the foundation since unforeseen limitations of the movements for the structure may be introduced.

The foundation is modelled with a characteristic element size of approximate 0.2 m, which is a considerably finer mesh than normally used for structural response modelling. A mesh refinement for the FE element at all locations of primary interest, and also for parts of the model that may influence the overall model response, is required to analyse stress concentrations e.g. close to the support areas and perforations. The selecting of correct areas for this mesh refinement is important to obtain detailed results. This increases the cpu-time for the simulations considerably. Furthermore, the local geometry of the supports is not described in detail, and as a result any stress concentrations due to the anchoring of the steel parts acting as support for the generator are not included in the analysis.

Future FE analyses may be validated by comparison with the measured response for a specific hydropower unit. These data should include vibration measurements of vibrations for the concrete foundation, and of forces acting on the concrete foundation. For validation purposes it is also necessary to include measurements of the stator, the generators supporting structure, etc.

7 Conclusions

Given the data presented in this report, it is evident that the loads from the turbine, generator and supporting structure which act on the concrete structure are dependent on the unit's design criteria and its present conditions. General conclusions are hard to draw from this initial analysis of one hydropower unit, since all units needs to be assessed individually. The performed analyses show an influence of the foundation properties on the behaviour of the generator. It is evident that this simplified FE model cannot accurately describe the structural interaction between generator and foundation. It is therefore necessary to perform enhanced analyses using considerably more detailed FE models to obtain quantified analyses results.

7.1 Design aspects and fault cases

At the generator, temperature variations cause shape deviations in the stator and supporting structure. The structures that are thermally reformed are heavy duty steel structures; this means that high forces act on the concrete unless the interconnection between the concrete and the steel structures is designed to manage these thermal movements.

The temperature variations near the turbine are small, but hydraulic properties at the runner cause high static and dynamic forces in certain operating modes. These forces are propagated to the concrete structure via a turbine guide bearing and the supporting structure.

Forces caused by mechanical and electrical unbalances occur in the case of all interconnections between the concrete structure and the unit components. If the unit is maintained correctly, these forces are in most cases considerably lower than the thermal and hydraulic loads.

The detailed design of the supporting structure's interconnection, loads under normal operation and in fault cases have to be known for the specific unit to perform an accurate analysis of the system.

7.2 Concrete foundation

The cracks in the foundation mainly influence the local stress levels in the concrete foundation due to the static load, i.e. gravity, with small influences shown for the dynamic response during normal operation. The redistribution of the forces within the concrete foundation results in increased maximum tensile stresses for the cracked foundations. Furthermore, local geometries changes, e.g. perforations, in combination with a cracked foundation may cause unfavourable stress concentrations. According to this it is necessary to accurately describe the properties of a concrete foundation to obtain reliable analysis results, incl. its connections to the surrounding structure and pre-existing cracks.

The resonance frequencies for the cracked foundation is as expected reduced compared to the un-cracked foundation, with the lowest frequencies being 30 and 25 Hz for the un-cracked and cracked foundation, respectively. However, the deformation modes relating to the lowest frequencies relates mainly to deformations of the upper part of the foundations, and not to the massive load bearing areas for the generator.

The concrete foundation with distributed cracks increases the radial support reactions for both the upper and lower generator bearing brackets during normal operation. The increases of the average support reactions for the guide bearing brackets are relative small, e.g. typically 3% to 4% increase for the model with distributed cracks compared to the intact foundation. However, the varied stiffness around the foundations results in varied maximum forces in different directions for the bearing brackets. This applies both to the un-cracked and cracked concrete foundations, but with considerably increased stress variations for the model with distributed cracks. Individual beams for the cracked model show increase of forces up to 14% and 7% for the upper and lower generator bearing brackets, respectively. The combination of anisotropic generator bearings, un-symmetric foundations, and distributed cracks may even further increase the variation of the reaction forces acting on the foundation. This creates uncertainties regarding the support reactions for the hydropower unit and also for the deformations of supports, since the foundation is not rigid.

Large loads on the concrete structure may occur in fault cases. If a short circuit occurs in the generator, high tangential loads occur at the stator's interconnection to the concrete. However, this type of load is seldom occurring. If entire or partial (uncontrolled) closing of guide vanes occurs at the turbine, high axial forces may act on the turbine cover due to water hammer. Furthermore, if the unit has disturbances which excite lateral natural frequencies, high radial forces may occur which act on all radial bearings' interconnections to the concrete structure. These may have a major impact on the magnitude of the support reactions acting on the concrete foundation. This increase of these support reactions is also likely to further increase the stresses for parts of the structure where high stresses already are localized, and also contribute to increased variations of the support reactions for bearing brackets. This needs to be further analysed with more detailed structural interaction models.

7.3 Future research

The combination of thermo-mechanical loads, drying shrinkage of concrete and dynamic response of the hydropower unit and concrete foundation needs to be analysed. Special attention should be given to the response of the system to different fault cases.

Localized stress concentrations in the concrete foundation need to be further analysed. The identifying of areas where crack initiation, or propagation of existing cracks, may occur is considered important within this type of study.

Future FE analyses of the hydropower generator and its structural interaction with the concrete foundation should incorporate anisotropic non-linear guide bearings, and detailed modelling of the connection points between supporting structure and supporting structure.

Analyses of concrete foundations with existing cracks are likely to contribute with deeper understanding of the behaviour of a cracked concrete foundation.

8 References

Belmans, R., Geysen, W., Jordan, H. and Vandenput, A. (1982). Unbalanced magnetic pull in three phase two pole induction motors with eccentric rotor. *Proceedings of IEE-International conference on Electrical Machines-Design and Applications*, pp. 65-69.

Gustavsson, R., Nässelqvist, M. and Berg, M. (2012). Measurement of rotor rim deformetions due to unsymmetrical air gap. *Proceedings of the 14th International Symposium on Transport Phenomena and Dynamics of Rotating Machinery,* Honolulu, Hawaii.

Hassanzadeh, M., Malm, R. and Nordström, E. (2012). Analysis of displacement and crack formations in foundations for hydropower generators. In: *24th ICOLD Congress,* 24 EME Congres De La CIGB, Kyoto. Q95-2.

Hillgren, N. (2011). *Analysis of hydraulic pressure transients in the waterways of hydropower stations.* Report no. UPTEC ES:11007, Uppsala University, Uppsala.

Larsson, M. (2010). *Fundament för vattenkraftgeneratorer - analys av krafter och deformationer.* LTU Report 2010:062 CIV, ISRN LTU-EX--10/062--SE, LTU, Luleå, 2010.

Malm, R., Hassanzadeh, M. Gasch, T., Eriksson, D. and Nordström, E. (2013). *Cracking in concrete supports for the generator in hydropower stations - Analyses of non-linear drying diffusion, thermal effects and mechanical loads*. Elforsk, Stockholm. (In press)

Nässelqvist, M. (2011). *Simulation and Characterization of Rotordynamic Properties for Vertical Machines,* ISBN 978-91-7439-360-6, Luleå University of Technology, Luleå.

Nässelqvist, M., Gustavsson, R. and Aidanpää, J. O. (2012). Bearing load measurement in a hydropower unit using strain gauges installed inside pivot pin. *Experimental mechanics*, *52*(4), 361-369.

Raabe, J. (1985). *Hydro power: the design, use, and function of hydromechanical, hydraulic, and electrical equipment*. VDI-Verlag, Düsserldorf.

Sadarangani, C. (2006). *Electrical machines-design and analysis of introduction and permanent magnet motors.* Royal institute of technology. Stockholm.

ELFORSK

SVENSKA ELFÖRETAGENS FORSKNINGS- OCH UTVECKLINGS - ELFORSK - AB

Elforsk AB, 101 53 Stockholm. Besöksadress: Olof Palmes Gata 31
Telefon: 08-677 25 30, Telefax: 08-677 25 35
www.elforsk.se